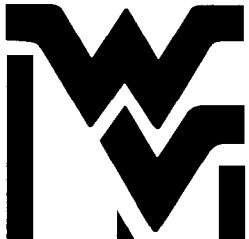

FRP Beam-Column Design Equations

Ever J. Barbero
127 Engineering Sciences Building
West Virginia University
Morgantown, WV 26506-6106

Mechanical and Aerospace Engineering Department

College of Engineering and Mineral Resources
West Virginia University • Morgantown, WV 26506-6106

TECHNICAL REPORT STANDARD TITLE PAGE

1. Report No.	2. Government Accession No.	3. Recipient's Catalog No.

4. Title and Subtitle	5. Report Date
FRP Beam-Column Design Equations	April 28, 2000
	6. Performing Organization Code

7. Author(s)	8. Performing Organization Report No.
Ever J. Barbero	

9. Performing Organization Name and Address	10. Work Unit No.
West Virginia University Morgantown, WV 26506-6106	11. Contract or Grant No. RP #131
	13. Type of Report and Period Covered

12. Sponsoring Agency Name and Address	13. Type of Report and Period Covered
West Virginia Department of Transportation Division of Highways 1900 Kanawha Blvd. East Charlestown, WV	Final
	14. Sponsoring Agency Code

15. Supplementary Notes

16. Abstract

A simple procedure was developed for the design of beam-columns. The design accounts for axial load eccentricity and lateral loads. Several examples are presented to illustrate the simplified design procedure. The procedure is also explained in the commentary. It was found that the section properties used in the design of beams and columns are sufficient for the design of beam-columns. No additional section properties are required. Therefore, the cost and time involved in testing structural shapes is minimized.

17. Key Words	18. Distribution Statement
FRP, composites	

19. Security Classif. (of this report)	20. Security Classif. (of this page)	21. No. of Pages	22. Price

NOTICE

The contents of this report reflect the views of the authors who are responsible for the facts and the accuracy of the data presented herein. The contents of this report do not necessarily reflect the official views or policies of the West Virginia Department of Transportation, Division of Highways, or the Federal Highway Administration. This report does not constitute a standard, specification, or regulation.

Contents

List of Figures

List of Tables

Executive Summary[1]

The objective of this report is to present a set of design equations for beam-columns made of pultruded fiber reinforced composite materials. A beam-column is a column subjected to a primary axial load and secondary bending load. The bending load may be caused by lateral loads or by eccentricity of the axial load (see Fig. 1).

This report is divided in the following sections:

1. Design procedure (Section 1). Describes the step-by-step design procedure to be followed to design fiber reinforced plastic (FRP) beam-columns. The procedure is based on four section properties which must be supplied by the manufacturer (see Tables 2-3). Testing procedures to be used in the experimental determination of those properties are available in the literature.

2. Examples (Section 2). The design procedure is illustrated with illustrative examples. These step-by-step examples make reference to the equations in the design procedure.

3. Commentary to the design procedure (Section 3). The commentary further explains the design procedure and provides justification for the equations presented.

4. Testing procedure (Section 4). It was found that no additional testing is required specifically for the design of beam columns. All the properties required for the design of beam columns are already available for the design of beams and columns without lateral load. Section 0.4 briefly describes the available literature where testing procedures are described for the determination of these properties.

5. Conclusions and recommendations. This section concludes the report and delineates some of the aspects that may need to be considered in the future.

[1] RP # 131

1 Design Procedure

The design of beam-columns begins by considering bending about the weak axis (Fig. 1). Then, the procedure is repeated to check bending about the strong axis.

A beam-column is a column subjected to a primary axial load and secondary bending load. Bending load may be caused by lateral loads or by eccentricity of the axial load. The design is based on four properties that should be provided by the manufacturer:

- The bending stiffness of the section (EI).
- The short-column buckling load P_L.
- The interaction constant c.
- The critical bending moment M_{cr}.

The design is carried out as follows:

1. Given the design load P_0, select a section with $P_L > P_0$ (see Table 2).
2. Compute the composite slenderness

$$\lambda = \frac{kL}{\pi}\sqrt{\frac{P_L}{(EI)}} \tag{1}$$

   where L is the length of the column (Figure 1) and k is the end-restraint coefficient (see Table 1). If $\lambda < 1$ the column is short, otherwise is long.

3. Compute the column load (no eccentricity, no lateral load)

$$P_c = k_i P_L \tag{2}$$

   where the interaction factor is

$$k_i = k_\lambda - \sqrt{k_\lambda^2 - \frac{1}{c\lambda^2}} \tag{3}$$

   where P_L and c are given in Table 2, and

$$k_\lambda = (1 + 1/\lambda^2)/2c \tag{4}$$

4. If only eccentricity of the axial load exists proceed to step 5. If lateral load exists, compute the equivalent end-moment M_0. The equivalent end-moment is such that it produces the same maximum deflection as the actual lateral load when no axial load is applied. That is

$$M_0 = 8\,(EI)\,\delta_{\max}/L^2 \tag{5}$$

where (EI) is the bending stiffness (Table 2) and $\delta_{\max}$ is the maximum deflection produced by the lateral load. Formulas used to compute $\delta_{\max}$ for a variety of cases are shown in Fig. 2.

5. Compute the reduced failure load

$$P_r = k_r P_L \tag{6}$$

in terms of the reduction factor k_r. Different reduction factors are used depending on the type of load, as follows:

(a) If the axial load has an eccentricity e, then

$$k_r = 0.871 - 0.0814(e/t) \tag{7}$$

where t is the flange thickness and e is the load eccentricity.

(b) If and end-moment M_0 results from lateral load, then

$$k_r = 1.001 - 1.012(M_0/M_{cr}) \tag{8}$$

where M_0 is the equivalent end-moment computed in step 4 and M_{cr} is the ultimate bending strength of the section acting as a beam (Table 2).

6. Compute the adjusted failure load (due to beam-column interaction)

$$P_a = k_a P_r \tag{9}$$

The adjustment factor k_a is computed as:

(a) For load eccentricity

$$k_a = 1.102 - 0.644\lambda \tag{10}$$

where λ is the composite slenderness (Eq. 1).

(b) For end-moment

$$k_a = 1.148 - 0.803\lambda \tag{11}$$

where λ is the composite slenderness (Eq. 1).

7. The adjusted failure load P_a should be lower than the design load P_0. If not, select another section. It is assumed that P_0 already contains load factors to account for uncertainty in the applied load. The factors k_r and k_a used in the determination of P_a are resistant factors that account only for variability of resistance of various structural shapes to sustain beam-column loads.

8. To check serviceability, first compute the reduced bending stiffness

$$(EI)_r = \left[(EI) - \left(\frac{kL}{\pi}\right)^2 P_0\right]\left(\frac{P_c}{P_E}\right) \tag{12}$$

where P_0 is the design load and P_E is the Euler load, computed as

$$P_E = \frac{(EI)}{(kL/\pi)^2} \tag{13}$$

The deflection is found considering only the lateral load and the true end conditions into the formulas in Fig. 2. For the load to be used in the equations, two cases are possible:

(a) For load eccentricity, use an end-moment equal to $M_0 = P_0 e$ where P_0 is the load and e is the eccentricity. For example, for a pinned-pinned column with load eccentricity, the lateral deflection is computed as

$$w = \frac{P_0 e L^2}{8(EI)_r} \tag{14}$$

(b) For lateral loads, use the actual load in terms of the reduced bending stiffness is $(EI)_r$ (see Example 3).

End-restraint	$\mathbf{K}_{theory}$	$\mathbf{K}_{steel}$	$\mathbf{K}_{wood}$
pinned-pinned	1.0	1.0	1.0
clamped-clamped	0.5	0.65	0.65
pinned-clamped	0.7	0.8	0.8
clamped-free	2.0	2.1	2.4

Table 1: End-restraint coefficients for long column buckling

SECTION	TYPE	(EI)weak	(GA)weak	P_L	c	Mcr
		in^2psi	in^2psi	lb		inlb
4x4x1/4	WF	1.03E+07	1.18E+06	51000	0.84	37732
6x6x1/4	WF	3.55E+07	1.83E+06	34000	0.84	48750
6x6x3/8	WF	5.19E+07	2.67E+06	111000	0.84	157830
8X8X3/8	WF	1.33E+08	3.78E+06	83000	0.84	161480
8X4X3/8	I	1.74E+07	1.94E+06	144000	0.84	70044
12x12x1/2	WF	5.26E+08	6.85E+06	157000	0.84	-

Table 2: Section properties provided by the manufacturer (Weak Axis)

SECTION	TYPE	(EI)strong	(GA)strong	P_L	c	Mcr
		in^2psi	in^2psi	lb		inlb
4x4x1/4	WF	3.08E+07	5.26E+05	51000	0.84	293,868
6x6x1/4	WF	9.92E+07	8.58E+05	34000	0.84	364,481
6x6x3/8	WF	1.54E+08	1.14E+06	111000	0.84	519,979
8X8X3/8	WF	4.06E+08	1.56E+06	83000	0.84	563,889
8X4X3/8	I	2.56E+08	2.21E+06	144000	0.84	1,060,648
12x12x1/2	WF	1.68E+09	3.28E+06	157000	0.84	-

Table 3: Section properties provided by the manufacturer (Strong Axis)

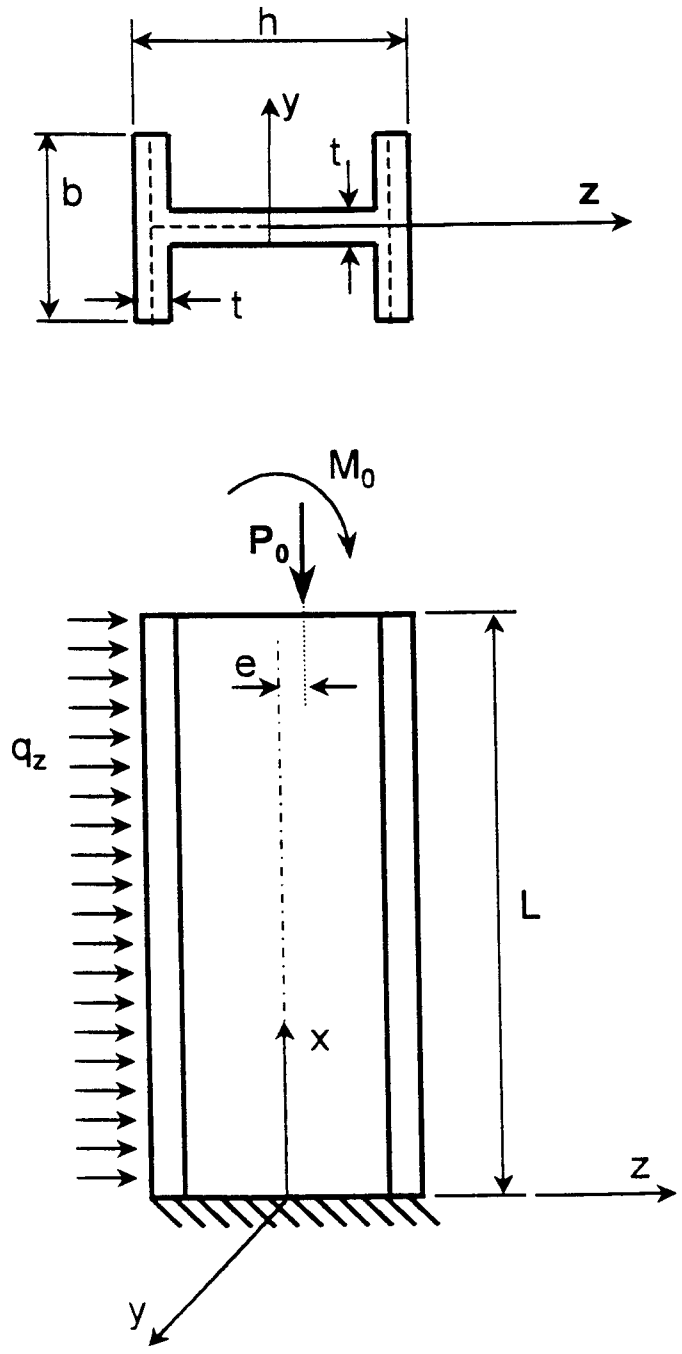

Figure 1: Coordinate system, dimensions, and loads for beam-column equations.

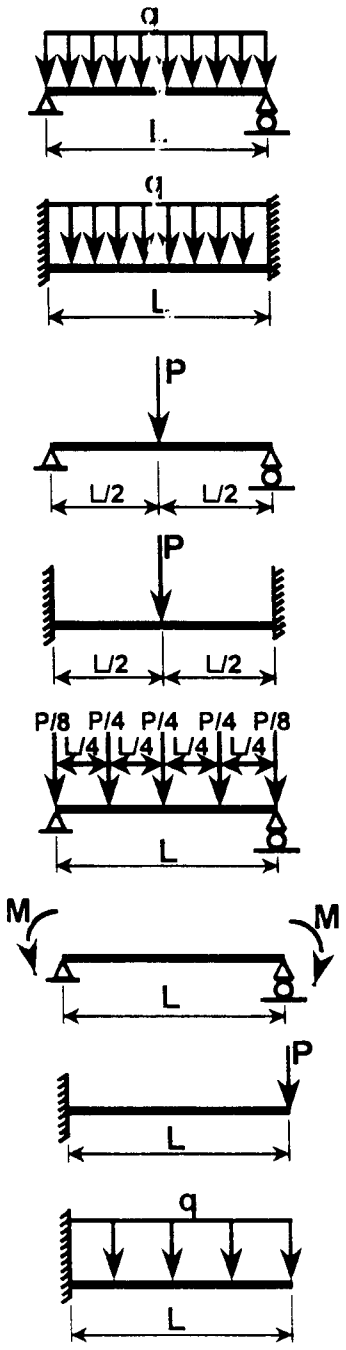

$$\delta_{max} = \frac{5}{384}\frac{qL^4}{EI} + \frac{1}{8}\frac{qL^2}{GA}$$

$$\delta_{max} = \frac{1}{384}\frac{qL^4}{EI} + \frac{1}{8}\frac{qL^2}{GA}$$

$$\delta_{max} = \frac{1}{48}\frac{PL^3}{EI} + \frac{1}{4}\frac{PL}{GA}$$

$$\delta_{max} = \frac{1}{192}\frac{PL^3}{EI} + \frac{1}{4}\frac{PL}{GA}$$

$$\delta_{max} = \frac{19}{1536}\frac{PL^3}{EI} + \frac{1}{8}\frac{PL}{GA}$$

$$\delta_{max} = \frac{ML^2}{8EI}$$

$$\delta_{max} = \frac{PL^3}{3EI} + \frac{PL}{GA}$$

$$\delta_{max} = \frac{qL^4}{8EI} + \frac{qL^2}{2GA}$$

Figure 2: Formulas to compute maximum lateral deflections of FRP beams subject to a variety of load and support conditions.

2 Examples

Example 1 *(Column) Select a section given the following:*

$P_0 = 80$ kip (Applied axial load)
$M_y = 0$ (Applied end-moment weak axis)
$M_z = 0$ (Applied end-moment strong axis)
$L = 72$ in (column length)
Ends: both pinned
$q_y = 0$ (Lateral load weak axis)
$q_x = 0$ (Lateral load strong axis)
$e = 0$ (Eccentricity of he axial load)

Solution 1 *Follow closely the design procedure described in Section 1:*

1. From Tables 2, select section with $P_L > P_0$. Select (Trial 1) $8 \times 8 \times 3/8$:

$$\begin{aligned} P_L &= 83.000 \text{ lb} \\ (EI)_w &= 1.33(10^8) \text{ lb in}^2 \\ c &= 0.84 \\ t &= 0.375 \text{ in} \end{aligned} \tag{15}$$

2. Compute the composite slenderness Eq. 1. Use Table 1 for end-conditions factor $k = 1$.

$$\lambda = \frac{kL}{\pi}\sqrt{\frac{P_L}{(EI)_w}} = 0.579 < 1 \text{ (short column)} \tag{16}$$

3. No lateral load, use Eq. 2 and Eq. 3

$$k_\lambda = (1 + 1/\lambda^2)/2c = 2.370 \tag{17}$$

$$k_c = \left[k_\lambda - \sqrt{k_\lambda^2 - \frac{1}{c\lambda^2}}\right] = 0.933 \tag{18}$$

$$P_c = 0.933 P_L = 77{,}439 \text{ lb} \tag{19}$$

4. $P_c < P_0$ (not adequate).

5. (Trial 2)$12 \times 12 \times 1/2$ WF/CP:

$$\begin{aligned} P_L &= 157,000 \text{ lb} \\ (EI)_w &= 5.26(10^8) \text{ lb in}^2 \\ c &= 0.84 \\ t &= 0.5 \text{ in} \end{aligned} \tag{20}$$

results in

$$\begin{aligned} \lambda &= 0.396 \\ k_\lambda &= 4.391 \\ k_i &= 0.972 \\ P_c &= 0.972 P_L = 152,604 \text{ lb} \end{aligned} \tag{21}$$

6. $P_c > P_0$ (adequate). Use: WF/CP $12 \times 12 \times 1/2$.

7. Verify strong axis load following same procedure.

Example 2 *(Load eccentricity) Select a section given the following:*

$P_0 = 20,000$ lb
$e = 0.5$ in (load eccentricity with respect to weak axis)
$L = 72$ in
Ends: both pinned
$M_y = M_z = q_y = q_z = 0$

Solution 2 *Follow closely the design procedure described in Section 1:*

1. From Table 2, select section with $P_L > P_0$. Select (Trial 1) $6 \times 6 \times 1/4$:

$$\begin{aligned} P_L &= 34,000 \text{ lb} \\ (EI)_w &= 3.55(10)^7 \text{ lb in}^2 \\ c &= 0.84 \\ t &= 0.25 \text{ in} \end{aligned} \tag{22}$$

2. Composite slenderness Eq. 1. Use Table 1 for end-conditions factor $k = 1$.

$$\lambda = 0.709 \tag{23}$$

3. Column buckling load. Eq. 2 and Eq. 3

$$\begin{aligned} k_\lambda &= 1.779 \\ k_i &= 0.886 \\ P_c &= 0.886 P_L = 30,124 \text{ lb} \end{aligned} \tag{24}$$

4. Reduction factor for eccentricity Eq. 7

$$k_r = 0.871 - 0.0814(0.5/0.25) = 0.708 \tag{25}$$

Reduced buckling load

$$P_r = k_r P_c = (0.708)30.124 = 21,328 \text{ lb} \tag{26}$$

5. Adjustment factor (beam-column interaction) for column with eccentricity Eq. 10

$$k_a = 1.102 - 0.644(0.709) = 0.645 \tag{27}$$

Adjusted buckling load

$$P_a = k_a P_r = (0.645)21.328 = 13,757 \text{ lb} \tag{28}$$

6. $P_a < P_0$ (not adequate).

7. (Trial 2) Use $4 \times 4 \times 1/4$

$$\begin{aligned} P_L &= 51.000 \text{ lb} \\ (EI)_w &= 1.03(10)^7 \text{ lb in}^2 \\ c &= 0.84 \\ t &= 0.25 \end{aligned} \tag{29}$$

Repeat steps 3 to 6

$$\begin{aligned} \lambda &= 1.613 \\ k_\lambda &= 0.824 \\ k_i &= 0.353 \\ P_c &= (0.353)51.000 = 18.003 \text{ lb} \end{aligned} \tag{30}$$

8. $P_c < 20.000$ (not adequate).

9. (Trial 3) Use $6 \times 6 \times 3/8$

$$\begin{aligned} P_L &= 111.000 \text{ lb} \\ (EI)_w &= 5.19(10^7) \text{ lb in}^2 \\ c &= 0.84 \\ t &= 0.375 \text{ in} \end{aligned} \tag{31}$$

Repeat steps 3 to 6

$$\begin{aligned} \lambda &= 1.06 \\ k_\lambda &= 1.125 \\ k_i &= 0.671 \\ P_c &= (0.671)\ 111{,}000 = 74{,}481 \text{ lb} \\ K_r &= 0.708 \text{ (no change)} \\ P_r &= (0.762)\ 74{,}481 = 52{,}733 \text{ lb} \\ K_a &= 1.102 - 0.644\ (1.06) = 0.419 \\ P_a &= (0.419)\ 56{,}755 = 22{,}095 \text{ lb} \end{aligned} \tag{32}$$

10. $P_a > P_0$ (adequate).

11. Check serviceability. First, compute the Euler load Eq. 13

$$P_E = \frac{5.19(10^7)}{(72/\pi)^2} = 98.810 \text{ lb} \tag{33}$$

12. Next, compute the reduced bending stiffness Eq. 12

$$\begin{aligned} (EI)_r &= \left[5.19(10^7) - \left(\frac{72}{\pi}\right)^2 20.000\right]\left(\frac{74.481}{98.810}\right) \\ (EI)_r &= 31.206(10^6) \text{ lb in}^2 \end{aligned} \tag{34}$$

13. The moment produced by eccentricity is

$$M_0 = Pe = 20.000(0.5) = 10.000 \text{ in lb} \tag{35}$$

14. Compute deflection with deflection equation using Eq. 14

$$\delta_{\max} = \frac{M_0 L^2}{8(EI)_r} = 0.208 \text{ in} \tag{36}$$

For other end-conditions or lateral loads use customary maximum deflection formulas in terms of $(EI)_r$.

Example 3 *(Lateral Load) Select a section given the following:*

$P_0 = 20.000$ lb
$L = 60$ in
Ends: both pinned
$M_y = M_z = 0$
$q_y = 10$ lb/in (uniformly distributed load, weak axis)
$q_z = 0$
$e = 0$ in

Solution 3 *Follow closely the design procedure described in Section 1:*

1. From Table 2, select section with $P_L > P_0$. Select (Trial 1) $6 \times 6 \times 1/4$:

$$\begin{aligned} P_L &= 34.000 \text{ lb} \\ (EI)_w &= 3.55(10)^7 \text{ lb in}^2 \\ (GA)_w &= 1.83(10)^6 \text{ lb} \\ M_{CR} &= 48.750 \text{ in lb} \\ c &= 0.84 \\ t &= 0.25 \text{ in} \end{aligned} \tag{37}$$

2. Composite slenderness Eq. 1. Use Table 1 for end conditions $k = 1$.

$$\lambda = 0.591 \tag{38}$$

3. Column buckling load

$$\begin{aligned} k_\lambda &= 2.299 \\ k_i &= 0.929 \\ P_c &= 0.929 P_L = 31,586 \text{ lb} \end{aligned} \tag{39}$$

4. Equivalent end moment. First compute the maximum deflection caused by the uniform distributed load (Figure 2)

$$\begin{aligned} \delta_{\max} &= \frac{5}{384}\frac{qL^4}{(EI)} + \frac{1}{8}\frac{qL^2}{(GA)} \\ \delta_{\max} &= \frac{5}{384}\frac{10(60^4)}{3.55(10^7)} + \frac{1}{8}\frac{10(60^2)}{1.83(10^6)} \\ \delta_{\max} &= 0.048 + 0.002 = 0.05 \text{ in} \end{aligned} \tag{40}$$

Next compute the equivalent end-moment using Eq. 5

$$M_0 = \frac{(8)3.55(10^7)0.05}{60^2} = 3,944 \text{ in lb} \tag{41}$$

5. Reduced failure load (due to end-moment), use Eq. 8

$$\begin{aligned} k_r &= 1.001 - 1.012(3944/48750) = 0.919 \\ P_r &= 0.919 P_L = 31,246 \text{ lb} \end{aligned} \tag{42}$$

6. Adjusted failure load, use Eq. 11 for end-moment

$$\begin{aligned} k_a &= 1.148 - 0.803\lambda = 0.673 \\ P_a &= 0.673 P_r = 21,029 \text{ lb} \end{aligned} \tag{43}$$

7. $P_a > P_0$ (adequate). Note that P_a is barely larger than P_0. It is assumed that P_0 already contains load factors to account for uncertainty in the applied load. The factors k_r, and k_a used in the determination of P_a are resistant factors that account only for variability of resistance of various structural shapes to sustain beam-column loads.

8. Serviceability. First compute the Euler load using Eq. 13

$$P_E = \frac{3.55(10^7)}{(60/\pi)^2} = 97,325 \text{ lb} \tag{44}$$

Then compute the reduced bending stiffness using Eq. 12

$$(EI)_r = \left[3.55(10^7) - (60/\pi)^2 20,000\right]\left(\frac{31.586}{97.325}\right) = 9.154(10^6) \text{ lb in}^2 \tag{45}$$

The maximum lateral deflection of a pinned-pinned beam under uniformly distributed load is from Fig. 2

$$\begin{aligned} \delta_{\max} &= \frac{5}{384}\frac{10(60^4)}{9.154(10^6)} + \frac{1}{8}\frac{10(60^2)}{1.83(10^6)} \\ &= 0.184 + 0.002 = 0.186 \text{ in} \end{aligned} \tag{46}$$

3 Commentary

3.1 Composite Slenderness

Since FRP shapes have different moduli at various points of the cross-section, the geometrical properties such as slenderness $r = \sqrt{I/A}$, moment of inertia I, area A, and so on are not appropriate to describe the section. To solve this problem, mechanical properties such as bending stiffness (EI) are defined and no attempt is made to separate E from I. Along these lines, the composite slenderness was defined in ref. [4] as

$$\lambda = \frac{kL}{\pi}\sqrt{\frac{P_L}{(EI)}} \tag{47}$$

where L is the total length of the column. In addition P_L is the short-column load (Tables 2-3), and (EI) is the bending stiffness, either weak or strong axis (Tables 2-3). Both P_L and (EI) are section-properties supplied by the manufacturer. Values of end-condition factor k (see Table 1) should be chosen using engineering judgement because exact end-conditions are seldom known.

3.2 Column Failure Load

The column failure load of a column loaded along its axis, with no load eccentricity and no lateral load, is found as

$$P_c = k_i P_L \tag{48}$$

where the interaction factor k_i is

$$k_i = k_\lambda - \sqrt{k_\lambda^2 - \frac{1}{c\lambda^2}} \tag{49}$$

where c is the interaction constant, and

$$k_\lambda = k_\lambda = (1 + 1/\lambda^2)/2c \tag{50}$$

This was called a universal equation in ref. [4, 5, 6] because a single expression is used for any column length without distinction of short, intermediate, or long columns. A comparison between the Euler load (Eq. 13)

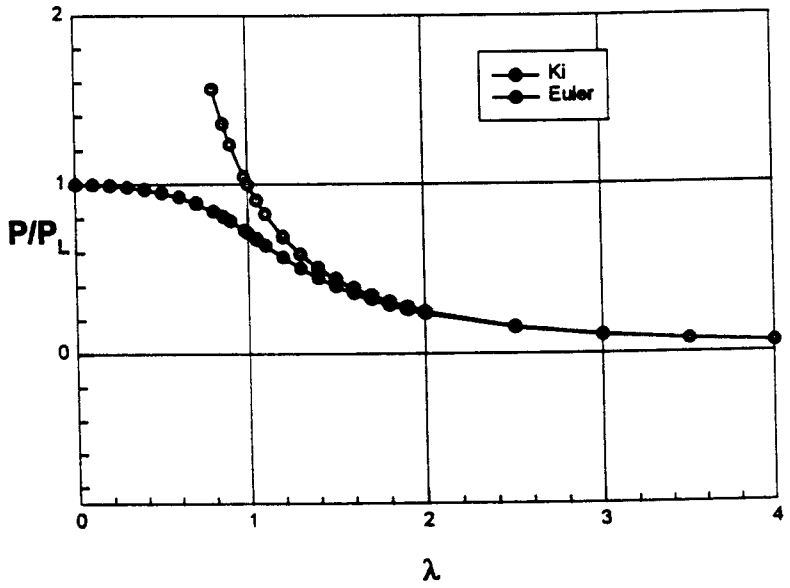

Figure 3: Comparison of buckling loads for columns without load eccentricity or lateral load.

and the actual column load given by Eq. 48 is shown in Fig. 3. Note that for $\lambda < 1$ the column load approaches the short-column load P_L as the column becomes shorter ($\lambda \to 0$). For experimental validation of these equations see ref. [4, 10].

3.3 Lateral Load

If the axial load P_0 is applied with some eccentricity e with respect to the axis of the column, an end-moment is produced, equal to

$$M_0 = eP_0 \tag{51}$$

Also, a column with lateral load q (Fig. 1) can be modeled as a column with end moments M_0 plus the axial load P_0. The equivalent end-moment

M_0 can be found for any type of lateral load and end conditions. The moment M_0 is such that produces the same maximum deflection on a pinned-pinned column as the actual lateral load acting on the column with actual end conditions. The maximum deflection δ_{max} under lateral load can be computed using Fig. 2 in terms of the bending stiffness (EI) and shear stiffness (GA), which are section-properties given by the manufacturer (see Tables 2-3).

For example, a clamped-clamped column with uniform lateral load (and no end load) deflects

$$\delta_{max} = \frac{qL^4}{384(EI)} + \frac{qL^2}{8(GA)} \tag{52}$$

Then, M_0 is found so that it matches the deflection of the actual column. Using the formula for the maximum deflection of a pinned-pinned beam under end moments (Fig. 2), M_0 is

$$M_0 = \frac{8(EI)\delta_{max}}{L^2} \tag{53}$$

3.4 Reduced Failure Load

Both eccentricity of the axial load and lateral load reduce the failure load of a column. The reduction factor depends of the source of end-moment.

(a) For eccentricity e

$$k_r = A_e - B_e(e/t) \tag{54}$$

(b) For end moment M_0

$$k_r = A_m - B_m(M_0/M_{cr}) \tag{55}$$

where t is the thickness of the flange and M_{cr} is the bending strength of the section working as a beam.

Then, the reduced failure load is

$$P_r = k_r P_L \tag{56}$$

The coefficients in Eqs. 54-55 (see Table 4) have been obtained from finite element modeling (FEM) of sections (listed in Tables 2-3) and further

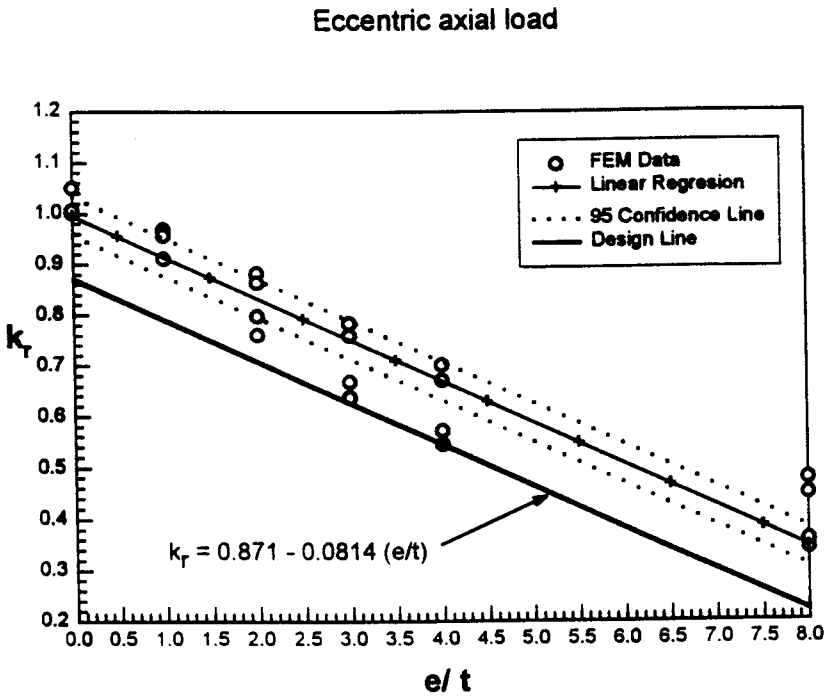

Figure 4: Resistance factor to account for load eccentricity

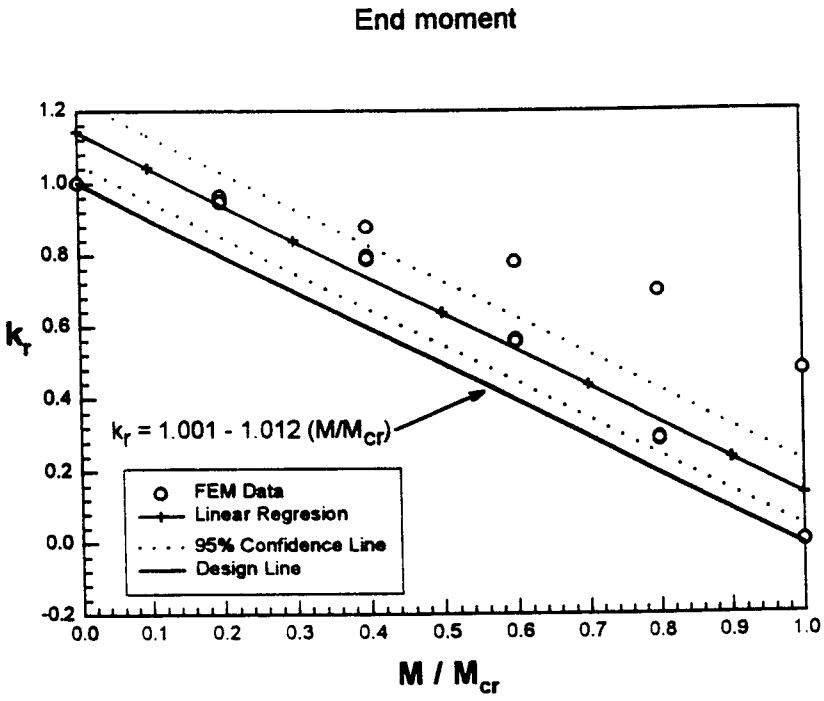

Figure 5: Resistance factor to account for end-moment

$\mathbf{A}_e$	0.871	$\mathbf{C}_e$	1.102
$\mathbf{B}_e$	0.0814	$\mathbf{D}_e$	0.644
$\mathbf{A}_m$	1.001	$\mathbf{C}_m$	1.148
$\mathbf{B}_m$	1.012	$\mathbf{D}_m$	0.803

Table 4: Design coefficients

validated experimentally. A comparison of Eqs. 54-55 with the data is shown in Fig. 4-5.

A linear regression provides a very good approximation of the relationship between k_r and e/t with a correlation coefficient of 92%. This means that 92% of the variability in the data is accounted for by the linear relationship. The remaining 8% is due to other unknown factors. Further support of a linear model is provided by a narrow 95 confidence interval. The 95% confidence lines drawn in the Fig. 4-5 mean that if the data were to be collected many times over, the linear regression line will be within the dotted lines 95% of the time. To account for all unknown factors, we decided to draw the design line parallel to the regression line and below all the data points available, as shown in Fig. 4-5.

The coefficients in Eq. 54 and 55 define a lower bound for the buckling load of a perfect column with eccentricity (or end-moment). Since a perfect column does not exist, the coefficients cannot be directly validated with experiments. However, they can be validated indirectly along with the coefficients defining k_a, as described below.

3.5 Adjusted Failure Load

The reduced failure load has to be further adjusted to account for imperfections, which leads to interaction between the lateral deflection and the local failure mode (e.g., flange buckling). This is accomplished by computing the adjustment factor k_a

(a) For eccentricity e

$$k_a = C_e - D_e\lambda \tag{57}$$

(b) For end moment M_0

$$k_a = C_m - D_m\lambda \tag{58}$$

Then, the adjusted failure load is Pa

$$P_a = k_a P_r = k_a k_r P_L \tag{59}$$

The coefficients in Eq. 57 and 58 (see Table 4) were obtained by linear regression of FEM data and validated experimentally. A comparison of Eq. 57 and 58 with the data is shown in Fig. 6-7. The linear regression provides a very good model for the relationship between k_a and λ as supported by a correlation coefficient of 87%. This means that only 13% of the variability in the data is not accounted by the regression. Also, the 95% confidence lines are close to the regression line, indicating good correlation between k_a and λ. Once more, to account for all factors, the design line was drawn parallel to the regression line but leaving all the FEM data above the line (see Fig. 6-7).

Note in Fig. 6 that all the experimental data are above the design line, thus validating the model. Note also that agreement between experiment and the linear model in Fig. 6 validate the linear model for k_r because the experimental failure loads were normalized by the theoretical value of P_r for plotting in Fig. 6.

The FEM was validated with experimental data obtained with $e = 0$ and $e = 1$" for several column types (listed in Tables 2-3) and several column lengths. Experimental and numerical values of load vs. lateral deflection are compared in Fig. 8. It can be seen that the actual lateral deflection (Euler mode) and the failure load are predicted accurately by the FEM model. Similarly, experimental and numerical values of load vs. flange deflections (local mode) are compared in Fig. 9, where good agreement between the experimental and numerical values in observed. Any discrepancies observed in the flange deflections are attributed to the variability of the imperfections in the sample tested. The experimental flange deflection was obtained by an optical measurement technique, which is described in [13, 10, 16]. All the details of the FEM modeling as well as all the experimental data are included in [16].

3.6 Interpretation of the Resistance Factors

The resistance factors k_a and k_r are used in Eq. 59 to estimate the failure load of the beam-column P_a. The value P_a does not account for uncertainties and/or variability in the design load. The failure load P_a is compared to the

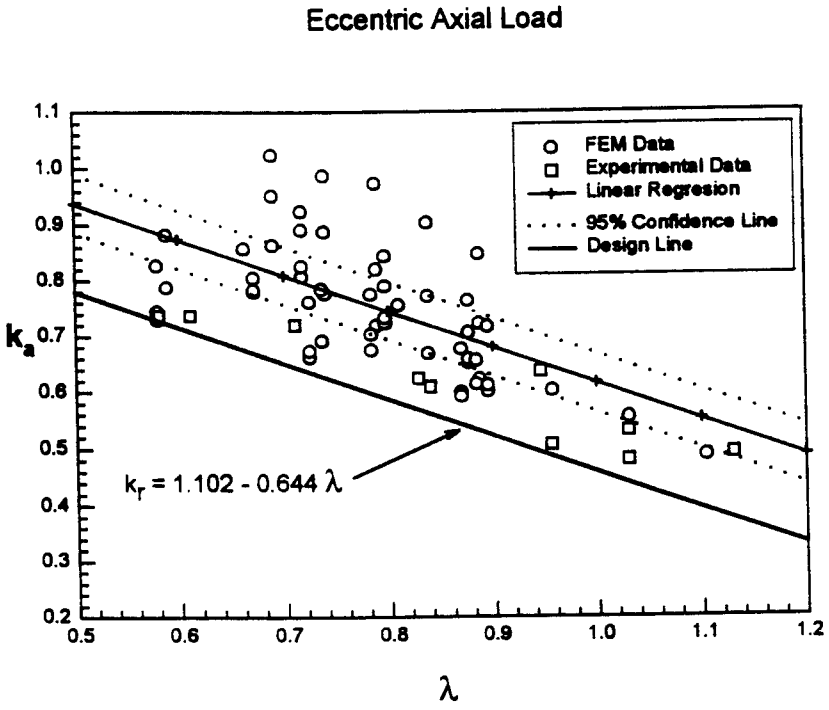

Figure 6: Resistance factor to account for beam-column interaction in the case of load eccentricity

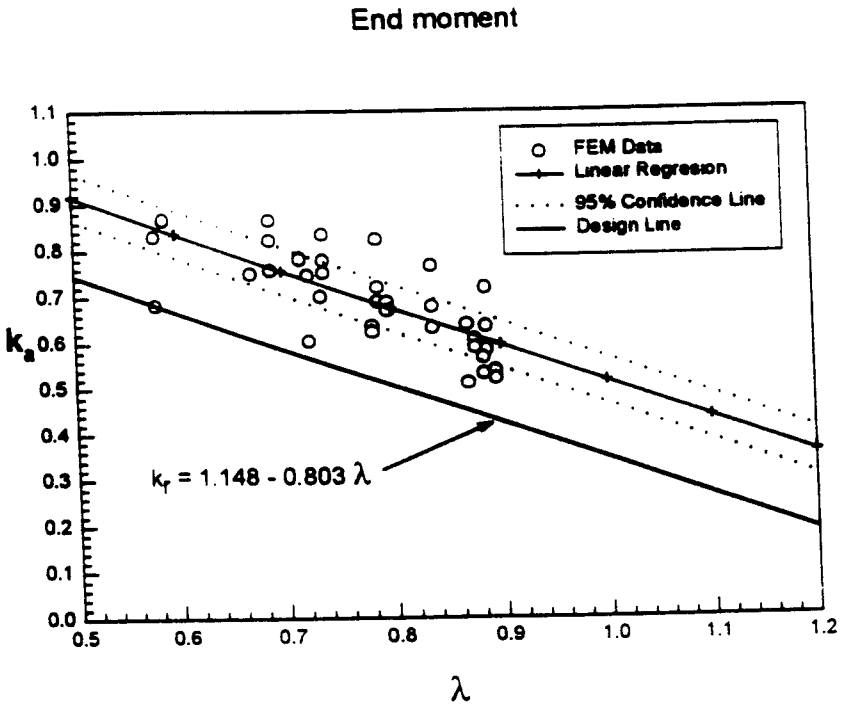

Figure 7: Resistance factor to account for beam-column interaction in the case of end-moment

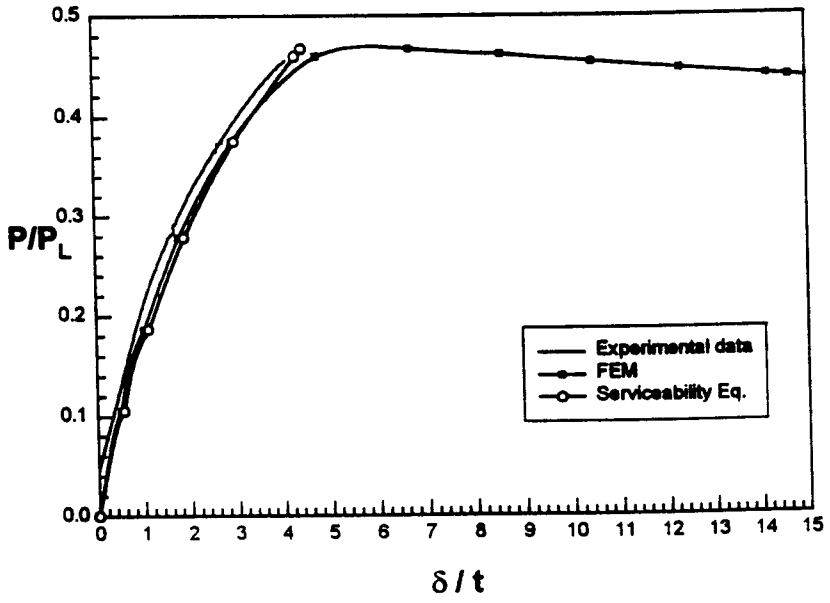

Figure 8: Load vs. lateral deflection of WF 8x8x3/8, L=132".

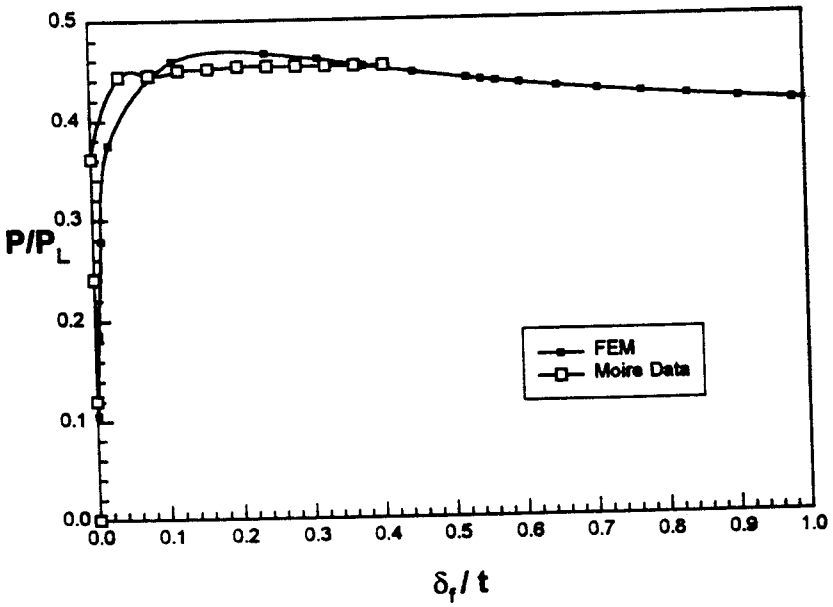

Figure 9: Load vs. flange deflection of WF 8x8x3/8, L=132".

design load P_0. It is assumed that the design load P_0 contains appropriate load factors to account for the variability and/or uncertainty in the applied load.

3.7 Serviceability

Even though the column may be able to carry the axial load, the resulting lateral deflection may be excessive. This is because the axial load effectively reduces the bending stiffness of the section, according to

$$(EI)_r = \left[(EI) - \left(\frac{kL}{\pi}\right)^2 P_0\right]\left(\frac{P_c}{P_E}\right) \tag{60}$$

where (EI) is the bending stiffness listed in Tables 2-3, k is the end-condition factor (Table 1), L is the column length, P_0 is the applied load, P_c is the column load (Eq. 48), P_a is the adjusted load (Eq. 59), $(EI)_r$ is the reduced bending stiffness (Eq. 60) and P_E is the Euler load computed as

$$P_E = \frac{(EI)}{(kL/\pi)^2} \tag{61}$$

Then, the lateral deflection of the column is computed as

$$\delta_{\max} = \frac{M_0 L^2}{8(EI)_r} \tag{62}$$

where M_0 is the end-moment computed as:

a - For eccentric load use Eq. 51

b - For lateral load use procedure leading to Eq. 53.

The serviceability equation (Eq. 60) was validated with experimental data as shown in Fig. 8, were excellent correlation is shown up to the failure point.

3.8 Weak and Strong Axis

The design is usually carried for the weak axis, until a section is selected. Then, the strong axis is checked following the same procedure by using the values in Table 3.

4 Testing Procedures

This section discusses the availability of data required for the design and the test procedures used to obtain such data.

The data necessary for design of beam-columns consists of:

- (EI): bending stiffness
- (GA): shear stiffness
- M_{cr}: bending strength
- P_L: short-column failure load
- c: interaction coefficient

Note that the design of beam-columns does not require any new property to be measured. The properties available for the design under pure bending and pure axial load are sufficient to complete the beam-column design. This is very advantageous because testing is expensive and time consuming.

4.1 Bending Test

A bending test is the simplest way of determining (EI), (GA), and M_{cr}. The testing procedure is described in detail in ref. [2] (see Appendix). These tests are done routinely by industry.

The values of (EI), (GA), and M_{cr} may be reported by industry in slightly different formats. For example, it is customary to divide the bending stiffness (EI) by I in order to report an apparent modulus E for the section. Such procedure has the disadvantage that different values of E are obtained from weak-axis and strong-axis bending tests, because the actual modulus E of the flanges and webs are different.

If the shear modulus G is reported instead of (GA), the area of the web only should be used for the computation of (GA). Using only the area of the web is customary practice in steel design. Theoretical support for this practice on composite sections can be found in [3, 8]. In any case, (GA) is used only to compute P_e which is only necessary in the serviceability equation (Eq. 60). Furthermore, the influence of shear deflections is very small, as shown in Example 3.

The value of M_{cr} should be obtained from test data. Predictions of M_{cr} using the flexure formula $\sigma = Mc/I$ [8] and the compressive strength of the material [7] are not accurate because the presence of some type of buckling during bending failure.

4.2 Short-Column Test

A short-column test provides the short-column failure load P_L. The test procedure is described in ref. [15] (see Appendix). This test is routinely done by industry.

The short-column load P_L is a section-property available in design manuals of all pultrusion manufacturers [14, 11, 9]. The value of P_L is usually controlled by local buckling of the flanges. The values listed in the design manuals have been determined by performing short-column tests such as those described in [15]. Material crushing may be also involved for sections with thick and narrow flanges. In this case the material failure is reflected in the value reported in the design manuals. However, the crushing load required to fail the material in compression without causing local buckling may be quite high. The crushing load can be predicted using equation (8.34) in [7]. Since the values of P_L reported by industry come from tests, they include the effects of both flange buckling and material crushing.

4.3 Interaction Constant

A column test of an intermediate length column is required to determine the interaction constant c. The length of the column is such that $\lambda = 1$ (Eq. 47). The test procedure is described in ref. [4] (see Appendix). The interaction constant c is used only in the serviceability equation (Eq. 60) or when no eccentricity and no lateral loads are present [4, 5, 6]. The use of the interaction constant c not only allows for accurate predictions of P_c but also greatly simplified the design by eliminating the need for considering separately the cases of short-, long- and intermediate-length columns.

When the value of the interaction constant c is not available, the designer may use engineering judgement to select a value. As it can be seen from Fig. 3, the effect of c in Eq. 48 is to create a smooth transition between the short-column load P_L and the Euler load (Eq. 61). When $c = 1$ the transition becomes sharp. In other words, when $c = 1$ an axially loaded column has either short- or long-column behavior; any intermediate-length

effect is denied. This type of behavior is not likely to occur, as indicated by experimental observations on composite columns [4, 10] and as well as steel [1, 12] and wood columns [17], both of which show distinctive intermediate-length effects. At the other extreme, a value of $c = 0$ means linear interaction (see Fig. 1 in [4]) and it is usually a conservative assumption. Since $c = 0$ cannot be used in Eq. 49 and 50, a very small value could be used instead. However, $c = 0$ is probably too conservative. The best option is to determine the value of c through testing, which is very simple [4, 10].

5 Conclusions and Recommendations

A simple procedure was developed for the design of beam-columns. The design accounts for load eccentricity and lateral loads. Several examples are presented in Section 2 to illustrate the simplified design procedure listed in Section 1. The procedure is also explained in the commentary (Section 3). It was found that no additional section properties are required for the design of beam columns. The section properties used in the design of beams and columns are sufficient. Therefore, the cost and time involved in testing structural shapes is minimized. Procedures for determination of those properties through testing of structural shapes are described in the literature, which is included in Appendix.

This project did not include long-duration loads, which may induce creep and stress-corrosion. Due to limitations of the testing equipment at the onset of the project, the larger sections introduced recently for bridge construction (e.g. $12\times12\times1/2$) were not tested. We have recently upgraded our equipment and we are now in a position to test those large sections if funding were available. Also, due to limited availability of samples, box-sections were not tested. With further collaboration with industry in the future we may be able to validate the proposed design method for closed sections.

Bibliography

[1] AISC ASD Design Manual, IX edition, 1989, American Institute of Steel Construction, Chicago, IL.

[2] Bank, L. C., Flexural and Shear Moduli of Full-Section Fiber Reinforced Plastic (FRP) Pultruded Beams, Journal of Testing and Evaluation, 17(1), 40-45, 1989.

[3] Barbero, E. J., Lopez-Anido, R.,and Davalos, J. F., On the Mechanics of Thin-Walled Laminated Composite Beams, Journal of Composite Materials, 27(8), 806-829, 1993.

[4] Barbero, E. J. and Tomblin, J. S., A Phenomenological Design Equation for FRP Columns with Interaction Between Local and Global Buckling, Thin-Walled Structures, 18, 117-131, 1994.

[5] E. J. Barbero, D. Evans, and S. Makkapatti, Buckling and Shear Tests Methods and Design Equations for Pultruded Shapes, NSF Sponsored First National Conference and Workshop on Research into Practice, Cristal City, VA, June 15-16, 1995.

[6] Barbero, E. J. and Evans, D., Guidelines for Design of FRP Columns, ASCE Structures Congress, Portland, OR, April 13-16, 1997.

[7] Barbero, E. J., Compressive Strength of FRP Materials, Final Report Task B4, Contract SPN T-699-FRP-1, West Virginia Division of Highways, 1998.

[8] Barbero, E. J., Introduction to Composite Materials Design, Taylor and Francis, Philadelphia, PA, Nov. 1998.

[9] BRP Design Guide, Bedford Reinforced Plastics, Inc., Bedford, PA, 1993.

[10] Dede, E., Experimental Validation of Buckling Mode Interaction in Intermediate Length Columns, Thesis, West Virginia University, Morgantown, WV., 1996.

[11] EXTREN Design Manual, Strongwell, Bristol, VA, 1994.

[12] Galambos, T. V., Guide to Stability Design Criteria for Metal Structures, Column Research Council, 4th ed. John Wiley, New York, 1988.

[13] Jones, S., Investigation of Local Buckling of Composite Columns by the Shadow Moire Method, Thesis, West Virginia University, Morgantown, WV., 1996.

[14] PULTEX Design Guide, Creative Pultrusions, Alum Bank, PA, 1989.

[15] Tomblin, J. S. and Barbero, E. J., Local Buckling Experiments on FRP Columns, Thin-Walled Structures, 18, 97-116, 1994.

[16] Turk, M., Experimental Investigation of Composite Beam-Column Behavior. Thesis, West Virginia University, Morgantown, WV., 1998.

[17] Zahn, J. J., Re-examination of Ylinen and other Column Equations-Interaction of Rupture and Buckling in Wood Members, ASCE J. Struct. Eng., 118(10) 2716-28, 1992.

Lawrence C. Bank[1]

Flexural and Shear Moduli of Full-Section Fiber Reinforced Plastic (FRP) Pultruded Beams

Authorized Reprint 1989 from Journal of Testing and Evaluation, January 1989

REFERENCE: Bank, L. C., "**Flexural and Shear Moduli of Full-Section Fiber Reinforced Plastic (FRP) Pultruded Beams,**" *Journal of Testing and Evaluation*, JTEVA, Vol. 17, No. 1, Jan. 1989, pp. 40–45.

ABSTRACT: An experimental methodology is presented for the simultaneous determination of the section flexural modulus and the section shear modulus of thin-walled fiber reinforced polyester and vinylester pultruded beams. A pilot test program, involving four different fiber reinforced plastic (FRP) beams, is described and results are discussed. A slenderness ratio is introduced to characterize the shape of the thin-walled beam, and recommended values of this ratio are suggested for design purposes. With available values of the section moduli the designer has the option of using the Timoshenko beam theory instead of the Euler-Bernoulli beam theory.

KEY WORDS: flexure testing, full-section testing, flexural modulus, shear modulus, fiber-reinforced plastics, pultruded beams, Timoshenko beam theory

Composite materials are continuing to see increased use in many engineering fields including that of structural engineering. Further increased use of composite materials in structural applications depends on cost and on designers, fabricators, and contractors becoming more familiar with composite materials and their behavior in structures.

The behavior of a composite structure depends on the mechanical properties of the structural elements that form the structure. The behavior of a structural element depends, in turn, on the mechanical properties of the composite material used in the structural element. On the micro-mechanical level the mechanical properties of the matrix and fiber constituents, their geometric relation to one another, and their volume fractions all enter into the characterization of the composite material. Much theoretical and experimental work has been done on characterizing the mechanical properties of various anisotropic composite materials [*1,2*].

In the analysis stage of design of a composite structure the designer must decide on the appropriate analytical method to use to model the structure [*3*]. Due to the complexity of the stress and strain distributions in composite materials the finite element method is often the only acceptable analytical tool for precise stress analysis. However, it is often desirable to use simplified analytical methods, especially for preliminary sizing and design. For two- or three-dimensional truss or frame structures the designer will often choose to use a rod or beam theory to model the structure. A choice must then be made as to which of the mechanical properties of the composite material to use in the structural model. Alternatively, the designer may decide to obtain the mechanical properties for the model from direct tests on the structural elements themselves. If the structural element has a complex internal structure or has mechanical properties that vary within the element itself, then tests on full-section structural elements may be the only way to obtain realistic design properties for a simplified structural model.

In this paper the use of full-section tests in characterizing the mechanical properties of thin-walled fiber reinforced composite material beams is investigated. Thin-walled composite material beams are being used in aerospace, mechanical, and civil engineering structures; see, for example, Refs *4* to *7*. In the aerospace and robotic fields composite material beams are usually custom designed and manufactured for very specific structural applications. Full-section element tests are performed to verify structural behavior that is predicted from analysis based on composite material properties. In the civil engineering field standard "off-the-shelf" thin-walled pultruded fiber reinforced plastic (FRP) beams are being produced in the United States for general purpose applications [*8,9*]. In the case of FRP standardized shapes, which are generally used as beams or beam columns, the manufacturers usually specify full-section stiffness properties for design purposes.

An experimental methodology is described which allows the simultaneous determination of the section flexural modulus and the section shear modulus of full-section beams for use in a shear deformation beam theory. The terminology "section" modulus is used to distinguish the measured property from the "material" or "coupon" modulus. The application to standard commercially produced pultruded fiber reinforced plastic beams is considered. Results of a pilot experimental program using pultruded FRP beams are described. Recommendations for testing FRP beams by the proposed method are given.

Beam Theory

If a beam theory is used to model the structural elements, the designer will need to obtain the relevant mechanical properties for the beam theory chosen. The choice of beam theory will depend on many factors, one of which is the degree of anisotropy of the composite material. Composite materials generally have ratios of their longitudinal modulus to their shear moduli which are higher than those for isotropic materials. Under these circumstances deformation of the beam due to shear will increase as this anisotropy ratio increases [*10*]. To account for this shear deformation the beam the-

Manuscript received 12/7/87; accepted for publication 7/20/88.

[1]Assistant Professor, Department of Civil Engineering, Rensselaer Polytechnic Institute, Troy NY 12180-3590. Currently: Department of Civil Engineering, The Catholic University of America, Washington, DC 20064.

0090-3973/89/0001-0040$02.50

ory due to Bresse and Timoshenko, generally called the Timoshenko beam theory [11], can be used as a first improvement over the Euler-Bernoulli beam theory, which does not account for shear deformation. In the Timoshenko beam theory two moduli are required. For isotropic materials these are the Young's modulus (E) and the shear modulus (G), and the deflection under static loads is found from the equations

$$EI\frac{\partial\phi}{\partial z} = M \tag{1}$$

$$\frac{\partial y}{\partial z} + \phi = \frac{Q}{kAG} \tag{2}$$

where I is the second moment of area, ϕ is the bending slope, z is the axial coordinate, M is the bending moment, y is the beam deflection, Q is the shear force, k is the shear coefficient, and A is the cross-sectional area. The shear coefficient k is a constant which accounts for the fact that the shear stress distribution is not uniform over the beam cross section. It depends on the cross-sectional shape, the material properties and, in dynamic analysis, on the frequency of vibration of the beam [12].

For anisotropic materials various anchors [e.g., 13-15] have considered the question of which of the anisotropic material constants are appropriate for use in the Timoshenko beam theory. Values of the shear coefficient have been given for a number of different anisotropic beams [16-18]. In this paper the Timoshenko beam theory is used to model a full-section beam element and as such is used in a macro-mechanical sense. For the full-section thin-walled beam element we define a section flexural modulus (E_b) and a section shear modulus (G_b) and write the two equations of the Timoshenko beam theory as

$$E_b I\frac{\partial\phi}{\partial z} = M \tag{3}$$

$$\frac{\partial y}{\partial z} + \phi = \frac{Q}{AG_b} \tag{4}$$

The full-section moduli depend on the geometrical and material properties of the thin-walled composite beam. It should be noted that the shear coefficient does not appear in Eqs 3 and 4 because it is incorporated into the section shear modulus which is now a mechanical property of the beam itself and not only a property of the material.

The moduli E_b and G_b can be found from direct tests on full-section beams by a procedure to be described in what follows. At first glance it may seem that the two moduli, especially the section shear modulus, would need to be obtained for every conceivable beam section for the formulation to be useful. In the case of a custom-made composite beam this is true, but in the case of pultruded FRP beams section shear moduli are found for families or types of the standard section profiles such as wide-flange, I beam, and rectangular box sections. It is known from analytical formulations [18,19] that the shear coefficient depends only on the relative dimensions of a thin-walled section and not on the absolute dimensions. Therefore all wide-flange sections made of the same composite material with the same microstructure, for example, would have the same value of k and therefore should have the same value of G_b.

Manufacturers of thin-walled pultruded FRP beams typically give only a value for the full-section flexural modulus for thin-walled FRP beams [8,9]. A single value of E_b is given for a given composite system, glass/polyester or glass/vinylester, which is intended for use with all shapes of cross sections. The flexural moduli are obtained from tests on long-span beams to obtain values that are unaffected by shear deformation during the actual testing. Since it is implicity assumed and is, in fact, suggested in the manufacturers' design manuals, that Euler-Bernoulli beam theory is to be used in design, the "given" value for the flexural modulus is actually lower than the true value. This "apparent" flexural modulus must be lowered to account for shear deformation effects in short-span beams and therefore it penalizes the designer of long-span beams. The use of a Timoshenko beam theory would allow much better utilization of FRP sections. The reason why this issue is so important for FRP beam sections is that many composite structural designs are deformation critical and not strength critical due to the low stiffness of pultruded fiber reinforced plastics [20]. The use of a more accurate theory would increase the competitiveness of FRP sections in relation to current construction materials.

Test Theory

Shear deformation has been recognized as an important influence on the test methods for obtaining the flexural modulus of composite materials [21]. Flexural modulus tests (ASTM D 790) for composite materials are performed on small solid rectangular cross-section beam coupons. A three-point bend or a four-point bend test configuration is used. The test is performed routinely because of its simplicity. The value of the flexural modulus obtained from the test is known to be different from the value of the longitudinal modulus for the same composite material found from a tensile test [22]. The test therefore really measures a structural/material mechanical property and not a pure material mechanical property as discussed in Ref 21.

For composite material solid rectangular test coupons it is recommended [21] that the ratio of the span length (ℓ) to beam height (h) be at least 60 for the effects of shear deformation to be negligible. For thin-walled sections the ℓ/h criterion cannot be used, since the height of the cross section is not the only geometrical property of importance. In fact, using such a criterion would imply that a 20 cm high I section would need to be tested over a span of 12 m. In such situations large deflections under small loads would create additional theoretical and experimental problems. The geometrical property used in this paper to characterize the thin-walled section is the ratio of the span length (ℓ) to the radius of gyration (r) about the bending axis. This "slenderness ratio" (ℓ/r) replaces the ℓ/h ratio as the parameter which determines the contribution of the shear deformation during the test.

The Timoshenko beam theory has been utilized previously by many authors [e.g., 21-23] to determine the flexural modulus of composite beams or for the simultaneous determination of the longitudinal and shear moduli of composite materials. The methodology proposed in this work follows that of Tolf and Clarin [22] but applies the concept to the testing of full-section thin-walled composite beams and the measurement of full-section flexural and shear moduli. For the three-point bend test configuration, Eqs 3 and 4 are solved to give

$$w = \frac{P\ell}{4}\left(\frac{\ell^2}{12E_bI} + \frac{1}{AG_b}\right) \tag{5}$$

where w is the midspan (maximum) deflection and P is the midpoint load. Equation 5 can be rewritten as

$$\frac{4Aw}{Pl} = \frac{1}{12E_b}\left(\frac{l}{r}\right)^2 + \frac{1}{G_b} \tag{6}$$

Equation 6 is an equation of a straight line where the slope and the intercept are directly related to the section flexural modulus and the section shear modulus, respectively. The slenderness ratio l/r appears as the independent variable and the quantity $4Aw/Pl$ as the dependent variable. Since shear deformation is accounted for in this experimental method, precise values can be obtained from tests on short-span beams.

In Ref *21* a substantial discussion is devoted to the effect of fiber eccentricity on the magnitude and distribution of the stresses in the small solid rectangular test coupon of composite material. Minor variations in fiber placement in parts of the beam cross section, which will inevitably be caused by the pultrusion process, will not affect significantly the overall properties of the beam section. This is due to the size of the cross section of the full-section specimen, which is much larger than that of the solid specimen: therefore local material inhomogeneities will have a smaller influence on the measured properties. In a similar investigation on braided composite I beams [*6*] the neutral surface was found to be very close to the center line of the beam.

The slenderness ratio can be used also to determine the span length required in a test setup to obtain the section flexural modulus from a test method that does not account for shear deformation. The apparent section flexural modulus (E_a) is related to the true section flexural modulus (E_b) and the slenderness ratio (l/r) by the formula

$$\frac{1}{E_a} = \frac{1}{E_b}\left(1 + 12\frac{E_b/G_b}{(l/r)^2}\right) \tag{7}$$

As can be seen the apparent section flexural modulus is always lower than the true section flexural modulus. For larger slenderness ratio values and for lower anisotropy ratios (E_b/G_b), the apparent section flexural modulus approaches the true section flexural modulus. Therefore, if the anisotropy ratio is known, one can determine the required slenderness ratio such that the percentage difference between the apparent and the true section flexural moduli is within some acceptable limit, for example, 5%. As shown in the test results that follow, the anisotropy ratio for typical pultruded FRP beams varies from 18 to 30. These values are significantly higher than those that would be found for beams of isotropic material.

Test Method

The FRP beam is tested in the three-point bend configuration. Since the test is performed on a full-section beam specimen, it is not the ASTM D 790 test which applies to a solid rectangular coupon. The underlying philosophy of this test is, however, the same as that of the three-point bend test in ASTM D 790. The beam is loaded at the midpoint, and the deflection at a point directly under the load is measured. In application of Eq 6 the beam is tested for a number of different spans. At each different span the beam is loaded quasi-statically to a nominal load (P) and the deflection (w) is measured. Theoretically, only two different spans are needed to obtain the two points required to characterize the straight line. However, taking measurements at a greater number of spans increases the number of experimental data points and reduces error. The straight line is then obtained by a linear regression through the experimental points obtained by plotting the variable $4Aw/Pl$ against $(l/r)^2$ as indicated in Eq 6. The section flexural modulus is obtained from the slope of the straight line, and the section shear modulus is obtained from the intercept of the straight line:

$$E_b = \frac{1}{12 \times \text{slope}} \tag{8}$$

$$G_b = \frac{1}{\text{intercept}} \tag{9}$$

Test Program

A pilot test program was conducted using four different 914 mm (36 in.) long commercially produced pultruded FRP beams obtained from Morrison Molded Fiber Glass Company (MMFG).[2] Two 102 by 102 by 6.4 mm (4 by 4 by 1/4 in.) wide-flange (WF) beams and two 102 by 51 by 6.4 mm (4 by 2 by 1/4 in.) I beams were tested. These dimensions are given for the cross sections of the I and WF beams where the values refer to the total cross-sectional height (h) by flange width (b) by thickness (t). For the beams tested the thickness of the flanges and the webs were equal and as such the thickness is constant and given by one value only. Figure 1 shows the cross-sectional shapes of the test specimens. The section properties given in Ref *8* for the WF beams are $I = 3.31 \times 10^6$ mm^4 (7.94 in.^{4}) and $r = 42$ mm (1.66 in.); those for the I beams are $I = 1.83 \times 10^6$ mm^4 (4.40 in.^{4}) and $r = 39$ mm (1.54 in.). Of each beam section one of the beams was an E-glass fiber/isophthalic polyester resin (Extren series 500) and the other was an E-glass fiber/vinylester resin (Extren series 625). The fibers are a combination of unidirectional rovings and continuous strand mat arranged in proprietary pattern and having a 40 to 50% volume fraction.

The test setup consisted of supports with diameters of 38 mm (1.5 in.) and a load bar with diameter of 51 mm (2 in.) made from steel round stock. The radii of the supports and load bars were chosen based on the flange thickness of the beams tested following the general guidelines of ASTM D 790, in which the center load bar is typically larger than the supports in the three-point bend test. The supports were placed on 203 mm (8 in.) high steel I beams to raise them off the testing table of a Baldwin Universal Testing System. Load was indicated on the digital display panel of the testing machine. An AMES 212.5 dial indicator, manufactured by B.C. Ames Company (Waltham, Mass.), having a sensitivity of 0.00254 mm (0.0001 in.), was placed directly under the load and deflections were recorded during the test. A photograph of the experimental rig is shown in Fig. 2.

Each beam was tested over spans having values of $(l/r)^2$ which started at 100 and increased in increments of 50 to 450 for both the WF and the I beams. The deflections were recorded for two different values of load: 3558 N (800 lb) and 5338 N (1200 lb) for the I beam and 4448 N (1000 lb) and 6672 N (1500 lb) for the WF beam. Each test was repeated twice so that four values were obtained for

[2]All measurements were made in standard U.S. units and then converted to SI units. For this reason the data in the figures appear in standard U.S. units. The mention of MMFG by name is only done to enable identification of the beams being tested and does not constitute any endorsement of the company or its products.

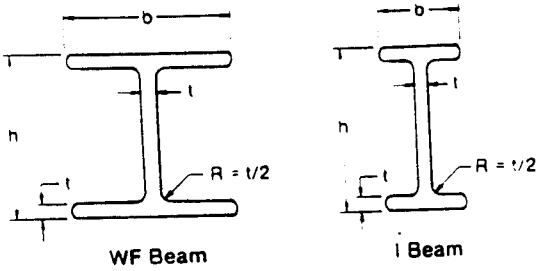

FIG. 1—*Geometrical specifications of the beam test specimens.*

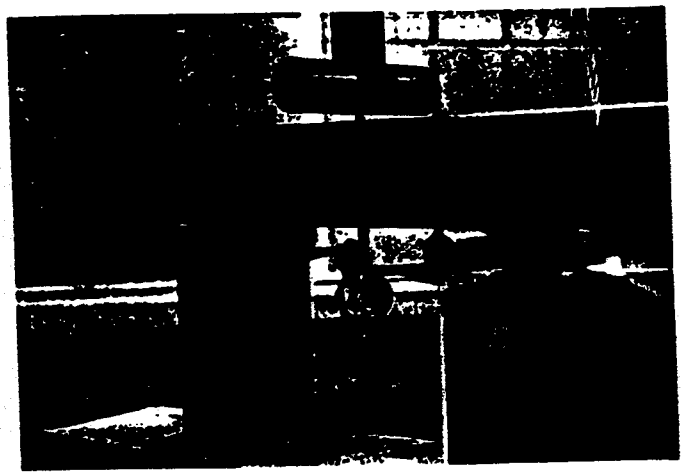

FIG. 2—*Test rig.*

the ratio P/w for each span. Values of the loads were chosen to give measurable deflections for each beam, while still remaining in the linear load-deflection range. However, the maximum deflections under the loads were always less than $\ell/330$. As such, the deflections were small enough so as not to require any corrections (ASTM D 790). The average of the four $4Aw/P\ell$ values was plotted against $(\ell/r)^2$ and the straight line graph drawn for each beam. Values of the slopes and intercepts were obtained from a computer graphics package which performed the linear regression.

Test Results and Discussion

Results of the tests are shown in Fig. 3 for the I beams and in Fig. 4 for the WF beams. Values of the slopes, intercepts, and correlation coefficients for the graphs shown in Figs. 3 and 4 are given in Table 1. Values of E_b and G_b for each beam calculated from the data in Table 1 are given in Table 2. The ratio E_b/G_b is also shown in Table 2 for each beam.

From Figs. 3 and 4 we see that the data points do, in fact, fall on a straight line. This is confirmed by the values obtained for the correlation coefficients. Even for points at $(\ell/r)^2$ equal to 100 the points do not deviate significantly from the straight line. The slope and the intercept of the straight line can be seen clearly. The differences between the response of the I and WF beams and the polyester and vinylester resin systems are seen.

The values of the flexural moduli shown in Table 2 fall into the range of flexural moduli expected for these beams. In Ref *8* the values of E_b suggested for design with the polyester and the vinylester resin fiber reinforced beams are 15.9 GPa (2.3 Msi) and 17.2 GPa (2.5 Msi), respectively. From Table 2 we calculate the average value of E_b for the polyester beams as 22.48 GPa (3.26 Msi) and for the vinylester beams as 22.34 GPa (3.24 Msi). Both values are higher than the recommended values. However, there does not seem to be a higher stiffness for the vinylester beams. In fact, as can be seen from Table 2 for the WF beams the flexural modulus of the vinylester beam is actually lower than that of the polyester beam.

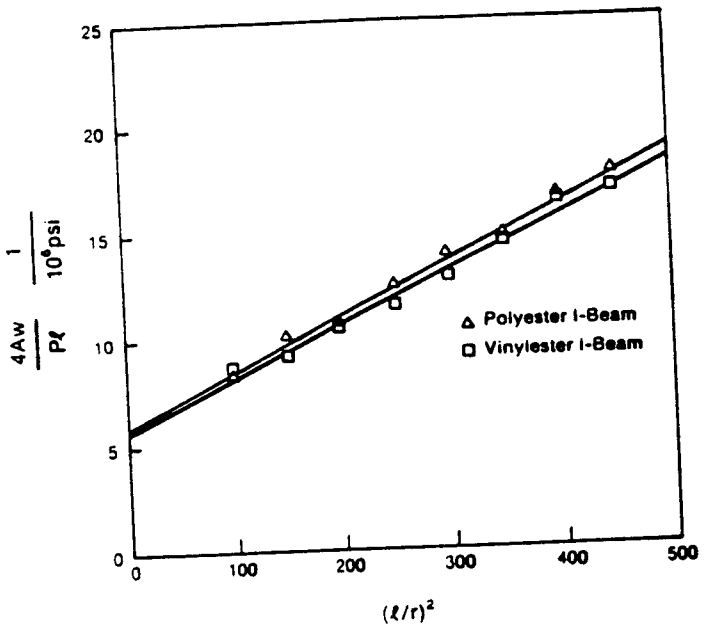

FIG. 3—*Test results for polyester and vinylester I beams (1 psi = 6895 Pa).*

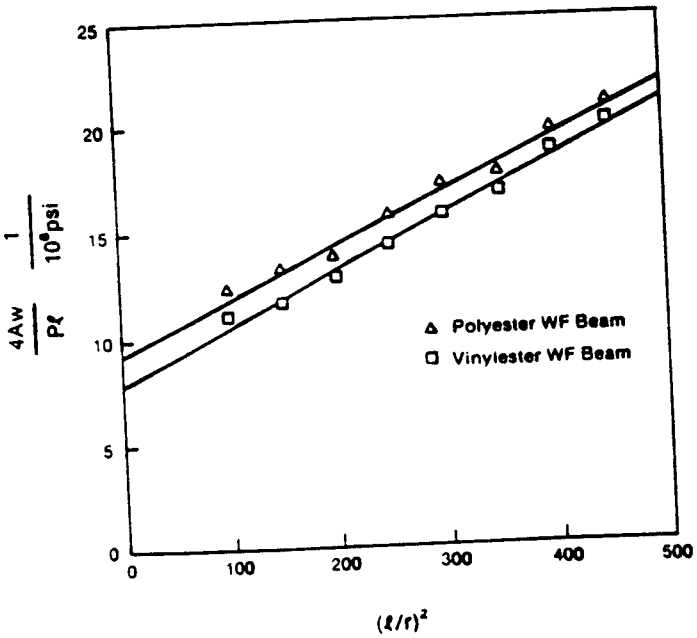

FIG. 4—*Test results for polyester and vinylester WF beams (1 psi = 6895 Pa).*

TABLE 1—*Values of slopes, intercepts, and correlation coefficients from linear regressions for four beam tests.*[a]

Beam	Slope ($\times 10^{-6}$) (psi^{-1})	Intercept ($\times 10^{-6}$) (psi^{-1})	Correlation Coefficient
I beam polyester	2.5933	5.7589	0.997
I beam vinylester	2.5183	5.5783	0.994
WF beam polyester	2.5233	9.2158	0.992
WF beam vinylester	2.6267	7.8042	0.994

[a]1 psi = 6895 Pa.

TABLE 2—*Results of tests on FRP beams.*[a]

Beam	E_b	G_b	E_b/G_b
I beam polyester	22.13 GPa (3.21 Msi)	1.20 GPa (0.174 Msi)	18.5
I beam vinylester	22.82 GPa (3.31 Msi)	1.23 GPa (0.179 Msi)	18.5
WF beam polyester	22.75 GPa (3.30 Msi)	0.75 GPa (0.109 Msi)	30.3
WF beam vinylester	21.86 GPa (3.17 Msi)	0.88 GPa (0.128 Msi)	25.6

[a]1 Msi = 6.895 GPa.

The section shear moduli show a clear difference between the values for the WF and the I beams. This confirms the fact that the section shear modulus is indeed a structural/material property. The trend towards the lower values of G_b for the wide-flange beams is expected, since these beams have much lower values of the shear coefficient [*18,19*] than do I beams. An examination of the actual values of the section shear moduli for the beams shows that there is a slight increase in G_b for the vinylester beams. This is also expected since the vinylester resin is somewhat stiffer than the polyester resin and we expect the resin properties to have more of an influence on the shear moduli than on the flexural moduli which are dominated by the fibers. Due to the lower values of G_b in the WF beams the ratios E_b/G_b for these beams are significantly higher than those for the I beams.

In Fig. 5 the values of E_b/G_b are used in Eq 7 to show the effect of shear deformation on the apparent flexural modulus, E_a. Figure 5 shows the ratio of E_a/E_b as a function of the slenderness ratio ℓ/r. As can be seen, for low values of ℓ/r the apparent flexural modulus is significantly lower than the true flexural modulus. The WF beams are more susceptible to shear deformation than the I beams. From the graphs in Fig. 5 we see that a slenderness ratio of 60 is required for all the beams to have less than a 10% error in the apparent flexural modulus and a slenderness ratio of 80 for this error to drop to 5%. For $\ell/r = 60$ the lengths of the WF and I beams required in order to neglect the effects of shear deformation are 2.53 m (8.3 ft) and 2.35 m (7.7 ft), respectively. Beams shorter than these lengths will have greater than 10% of their deflection due to shear deformation, and a shear deformation beam theory should be used in their design. For a 305 by 305 by 13 mm (12 by 12 by 1/2 in.) WF beam with $r = 129$ mm (5.07 in.) the required beam length for $\ell/r = 60$ is calculated to be 7.73 m (25.4 ft).

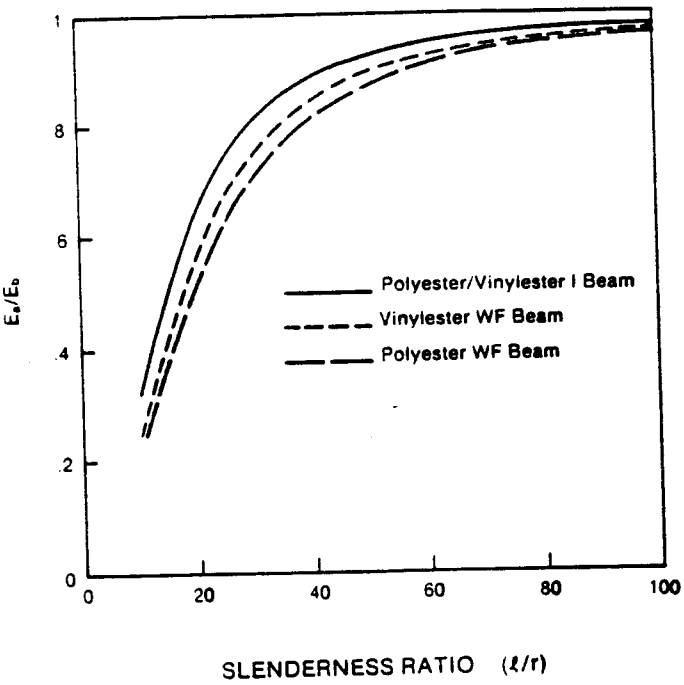

FIG. 5—*Ratio of the apparent flexural modulus to the true flexural modulus as a function of the slenderness ratio for the four beam tests.*

It is interesting to note that the requirement of $\ell/r = 60$ can be compared with the requirement for solid composite beam coupons [*21*] which is $\ell/h = 60$. The slenderness ratio for the testing of full section FRP beams seems justified and is useful for characterizing the response of beams susceptible to shear deformations.

Conclusion

A methodology has been presented for obtaining the section flexural modulus and the section shear modulus from tests on full-section thin-walled fiber reinforced plastic beams. Results of a pilot experimental investigation show that reasonable values are obtained for these moduli from the test method proposed. The use of the section moduli in a Timoshenko beam theory is suggested for designers. With available values of the section shear moduli the additional effort required to use the Timoshenko beam theory is minimal [*24*]. The payoff in better estimation of beam deflections should allow more realistic designs and cost savings.

Although the methodology proposed has concentrated on thin-walled sections of pultruded FRP the use of the test for thin-walled beams constructed of other composite material systems is also appropriate. For systems such as graphite/epoxy with higher anisotropy ratios the use of a shear deformation beam theory becomes even more important. An additional potential use for the test now being investigated is to obtain values for the shear coefficient for thin-walled composite beams [*18*]. Since $G_b = kG_{material}$, the test allows experimental verification of the material shear modulus or the shear coefficient. An extensive test program is currently investigating these and other phenomena associated with the behavior of thin-walled fiber reinforced plastic beams.

Acknowledgments

This work was performed under Contract RI-A-87-2 from the Engineering Foundation. The Morrison Molded Fiber Glass Company of Bristol, Virginia, supplied the beams. Undergraduate students V. Murray, D. Hammer, and K. Reed performed the experiments, and Instrumentation Engineer B. Mielke assisted with the equipment.

References

[1] Whitney, J. M., Daniel, I. M., and Pipes, R. B., "Experimental Mechanics of Fiber Reinforced Composite Materials," SESA Monograph No. 4, Prentice-Hall, Englewood Cliffs, N.J., 1982.

[2] Christensen, R. M., *Mechanics of Composite Materials*, Wiley-Interscience, New York, 1979.

[3] Vinson, J. R. and Sierakowski, R. L., *The Behavior of Structures Composed of Composite Materials*, Martinus Nijhoff, Amsterdam, 1987.

[4] Sung, C. K. and Thompson, B. S., "A Methodology for Synthesizing High-Performance Robots Fabricated with Optimally Tailored Composite Laminates," *ASME Journal of Mechanisms, Transmissions, and Automation in Design*, ASME Paper 86-DET-8, 1986.

[5] Bicos, A. S. and Springer, G. S., "Design of a Composite Boxbeam," *Journal of Composite Materials*, Vol. 20, 1986, pp. 86-109.

[6] Yau, S.-S., Chou, T.-W., and Ko, F. K., "Flexural and Axial Compressive Failures of Three-Dimensionally Braided Composite I-Beams," *Composites*, Vol. 17, 1986, pp. 227-232.

[7] Holmes, M. and Just, D. J., *GRP in Structural Engineering*, Applied Science, Essex, England, 1983.

[8] *Extren Fiberglass Structural Shapes Engineering Manual*, Morrison Molded Fiber Glass Company, Bristol, Va.

[9] *Design Guide*, Creative Pultrusions, Alum Bank, Pa.

[10] Dudek, T. J., "Young's and Shear Moduli of Unidirectional Composites by a Resonant Beam Method," *Journal of Composite Materials*, Vol. 4, 1970, pp. 232-241.

[11] Timoshenko, S. P., Young, D. H., and Weaver, W., *Vibration Problems in Engineering*, 4th ed., Wiley, New York, 1974.

[12] Kaneko, T., "On Timoshenko's Correction for Shear in Vibrating Beams," *Journal of Physics, D, Applied Physics*, Vol. 8, 1975, pp. 1927-1936.

[13] Nowinski, J. L., "On the Transverse Wave Propagation in Orthotropic Timoshenko Bars," *International Journal of Mechanical Sciences*, Vol. 11, 1969, pp. 689-694.

[14] King, J. L., "The Free Transverse Vibrations of Anisotropic Beams," *Journal of Sound and Vibration*, Vol. 98, 1985, pp. 575-585.

[15] Bank, L. C. and Bednarczyk, P. J., "Deflection of Thin-Walled Fiber Reinforced Composite Beams," in *Proceedings*, Second Technical Conference, American Society for Composites, 23-25 Sept. 1987, Newark, Del., Technomic Publishing Company, pp. 553-562.

[16] Dharmarajan, S. and McCutchen, H., Jr., "Shear Coefficients for Orthotropic Beams," *Journal of Composite Materials*, Vol. 7, 1973, pp. 530-535.

[17] Teh, K. K. and Huang, C. C., "Shear Deformation Coefficient for Generally Orthotropic Beam," *Fibre Science and Technology*, Vol. 12, 1979, pp. 73-80.

[18] Bank, L. C., "Shear Coefficients for Thin-Walled Composite Beams," *Composite Structures*, Vol. 8, 1987, pp. 47-61.

[19] Cowper, G. R., "The Shear Coefficient in Timoshenko's Beam Theory," *ASME Journal of Applied Mechanics*, Vol. 33, 1966, pp. 335-340.

[20] *Structural Plastics Design Manual*, ASCE Manuals and Reports on Engineering Practice No. 63, American Society of Civil Engineers, New York, 1984.

[21] Zweben, C., Smith, W. S., and Wardle, M. W., "Test Methods for Fiber Tensile Strength, Composite Flexural Modulus, and Properties of Fabric-Reinforced Laminates," in *Composite Materials: Testing and Design (Fifth Conference), ASTM STP 674*, S. W. Tsai, Ed., American Society for Testing and Materials, Philadelphia, 1979, pp. 228-262.

[22] Tolf, G. and Clarin, P., "Comparison Between Flexural and Tensile Modulus of Fibre Composites," *Fibre Science and Technology*, Vol. 21, 1984, pp. 319-326.

[23] Fischer, S., Roman, I., Harel, H., Marom, G., and Wagner, H. D., "Simultaneous Determination of Shear and Young's Moduli in Composites," *Journal of Testing and Evaluation*, Vol. 9, No. 5, 1981, pp. 303-307.

[24] Bank, L. C. and Bednarczyk, P. J., "A Beam Theory for Thin-Walled Composite Beams," *Composites Science and Technology*, Vol. 32, 1988, pp. 265-277.

Thin-Walled Structures 18 (1994) 97–116

Local Buckling Experiments on FRP Columns

John Tomblin & Ever Barbero

Mechanical and Aerospace Engineering, Constructed Facilities Center, West Virginia University, Morgantown, WV 26506-6101, USA

(Received 31 July 1991; revised version received 3 March 1992; accepted 16 June 1992)

ABSTRACT

In this paper, local flange-buckling of thin-walled pultruded FRP columns is investigated. Experimental data are presented and correlated with theoretical predictions. Good agreement between theoretical and experimental results is found. Possible explanations for slight deviations in the experimental data are advanced. The experimental and data reduction procedures used to obtain the local buckling loads are presented. A new data reduction technique using Southwell's method is developed to interpret local buckling test data. The usefulness of the data reduction technique is demonstrated for various column sections and experimental conditions.

1 INTRODUCTION

Pultruded composite beams and columns are being extensively used for civil engineering structural applications. They have many advantages over conventional materials (steel, concrete, wood, etc.), such as light weight and high corrosion resistance. Mass production of composite structural members (e.g. by pultrusion) makes composite materials cost-competitive with conventional ones. In the pultrusion process, fibers and polymer resin are pulled through a heated die that provides the shape of the cross-section to the final product. Pultrusion is a continuous process for the production of prismatic sections of virtually any shape.[1] Other mass production techniques like automatic tape layout can also be used to produce prismatic sections.

Thin-Walled Structures 0263-8231/94/$07·00
Printed in Great Britain.

Pultruded structural members have open or closed thin-walled cross-sections. For long composite columns, overall (Euler) buckling is more likely to occur before any other instability failure. For short columns, local buckling occurs first, leading either to large deflections and finally to overall buckling or to material degradation due to large strains (crippling). For intermediate lengths, interaction between local and global buckling and possibly material degradation may occur. Because of the large elongation to failure allowed by both the fibers and the resin, the composite material remains linearly elastic for large deflections and strains, unlike conventional materials that yield (steel) or crack (concrete) for moderate strains. Therefore, buckling is the governing failure for this type of cross-section and the critical buckling load is directly related to the carrying capacity of the member.

For a composite column, the classical buckling theory[2] in combination with basic concepts of the classical lamination theory[3,4] are applied in order to determine the bending stiffness of the column[5] and the critical buckling load.[6] In the case of short columns, Euler's theory cannot be applied because short column buckling failure is associated more likely with local buckling (i.e. buckling of a part of the cross-section of the column) or material failure that may be encountered before any instability failure. A very short column of solid cross-section with thin parts, such as wide flange I-beams and box beams, is considered herein.

The problem of local buckling has already been considered for steel cross-sections and considerable research has been done in this area in order to increase the carrying capacity of a steel member against local buckling by introducing stiffeners.[7] An analytical solution for local buckling of pultruded composite columns[6] is used in this work. Other alternatives are to use the Finite Strip method[8] or the Finite Element Method.[9] Experimental results on FRP columns for cooling towers were presented by Yuan.[10]

In almost any experimental test, the validity of the test somewhat relies on the workmanship of the testing apparatus and material being tested. This is particularly true in a buckling test where a high state of instability exists. Due to the manufacturing process of pultruded fiber reinforced plastic (FRP) beams, imperfections in the final beam composition are impossible to control to any reliable estimate. These imperfections will play a large role in any buckling experiment.

2 DATA REDUCTION IN LONG-COLUMN BUCKLING

This section provides the background for the proposed data reduction method for local buckling described in Section 3. In any buckling experi-

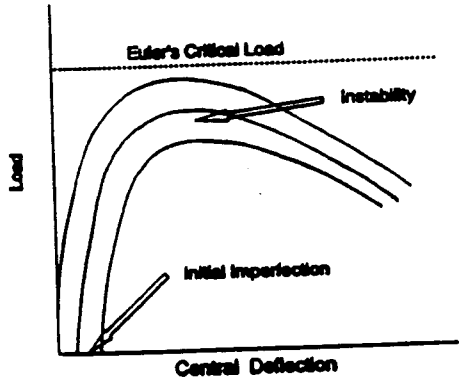

Fig. 1. Experimental curves for a column with initial imperfections.

ment, particularly one using FRP sections, the theoretical critical load of the column is almost never achieved due to material imperfections. The resulting load–deflection curve will have the form represented in Fig. 1. Its maximum is very difficult to obtain experimentally and it may not have a close correspondence with the theoretical critical load P_{cr}. Thus, it becomes necessary to make use of the method proposed by Southwell[11,12] which takes into account the load reduction resulting from such imperfections.

2.1 Southwell's method

The governing equation for an axially loaded column in terms of the deflection w and an imperfection w_o, both measured from the line of application of the load, is

$$D\left(\frac{d^2w}{dx^2} - \frac{d^2w_o}{dx^2}\right) + Pw = 0 \tag{1}$$

Provided that w_o vanishes at each end of the column, a general solution of eqn (1) may be obtained by expressing w and w_o in terms of a Fourier series, assuming w and w_o will be continuous functions of x:

$$w = \sum_{n=1}^{\infty}\left[A_n \sin\frac{n\pi x}{L}\right] \tag{2}$$

$$w_o = \sum_{n=1}^{\infty}\left[\overline{A_n} \sin\frac{n\pi x}{L}\right] \tag{3}$$

By substituting eqn (2) and (3) into eqn (1), the following relation is found:

$$A_n = \frac{\overline{A_n}}{1 - \frac{P}{P_n}} \tag{4}$$

where P_n represents the critical load of the nth mode. The true deflection measured with respect to the centroidal axis of the column (or middle surface of the flange) is $\Delta = w - w_o$. In the case of no interaction among modes, one modes dominates and Δ reduces

$$\Delta = \frac{\overline{A_1} \sin \frac{\pi x}{L}}{\frac{P_1}{P} - 1} \tag{5}$$

or

$$\frac{\Delta}{P} = \frac{1}{P_1} \Delta + \frac{\overline{A_1}}{P_1} \sin \frac{\pi x}{L} \tag{6}$$

Equation (5) relates the deflection Δ to the increasing load P. This equation also represents a rectangular hyperbola having the axis $\Delta = -\overline{A_1}$ and the horizontal line $P = P_1$ as asymptotes (Fig. 2). Equation (6) represents a linear relationship between Δ/P and Δ with the inverse of the slope representing the critical buckling load and the Δ-intercept representing the apparent imperfection (Fig. 3).

Southwell's method may also be extended to cases which also take into account real imperfections of the beam, eccentricity at the ends, the beam's own weight, and transverse lateral load,[13,14] all of which have the same effect when analyzed by Southwell's method. On all accounts, the load will not pass exactly through the centroid of the section and the column will be subjected to bending actions and lateral deflections from the first application of load. Southwell's method is extended in the next section for data reduction of local-buckling test data.

3 DATA REDUCTION IN LOCAL BUCKLING

Although Southwell's method was developed for the long column (Euler) case, application to short columns, tested in the manner described above, appears to be possible. As will be seen in following sections, measurements taken on the flanges during a local buckling test fall on the same hyperbolic curve as shown in Fig. 2. Thus, when this curve is linearized, the slope of the resulting straight line will give the inverse of the critical load as shown in Fig. 3.

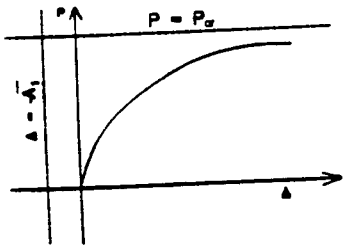

Fig. 2. Hyperbolic Δ–P plot with asymptotes $P = P_1$ and $\Delta = -\overline{A_1}$.

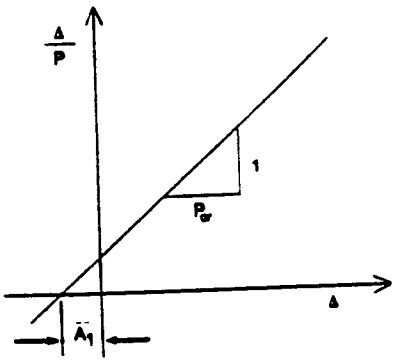

Fig. 3. Linearized Δ–Δ/P plot with slope $1/P_1$ and intercept $-\overline{A_1}$.

A major question in the application of the proposed data reduction method to the local buckling measurement is the placement of the gauges with respect to the buckled mode shape. As in the classical Southwell's method, the most logical gauge placement will be in the center of a buckling wave in the sample being tested (where the maximum deflection can be obtained with respect to the compressive load). But, in local flange buckling tests, the convenience of being able to properly place a gauge in the center of a wavelength is impossible due to the unknown buckled shape.

For example, a typical buckled flange with three gauges placed along the wavelength L' is shown in Fig. 4. Recalling eqn (6), the deflection is dependent upon the position x of the gauge with respect to the wavelength L'. Hence, with respect to Fig. 4, eqn (6) becomes

$$\frac{\Delta}{P} = \frac{1}{P_1}\Delta + \frac{\overline{A_1}}{P_1}\sin\frac{\pi x}{L'} \tag{7}$$

When this linear relation is plotted, the slope of the straight line is the inverse of the critical load $(1/P_1)$ and the intercept is the initial deflection

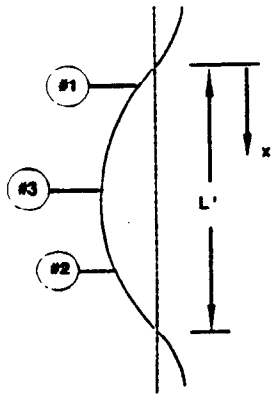

Fig. 4. Section of buckled flange with wavelength L'.

or imperfection, in this case $\overline{A_1}\sin(\pi x/L)$. When several gauges from the same test are linearized and placed on the Δ–Δ/P plot, the resulting lines will fall on lines similar to those represented in Fig. 5.

As shown in Fig. 5, even though all lines have different intercepts (different values of the wavelength position x), the slope remains constant at $1/P_1$. Hence, the critical load can be obtained regardless of the gauge position with respect to the wavelength. This is very important because of the following: if only one displacement transducer is available, its output can be used regardless of its location with respect to the unknown location of the maximum deflection of the buckled flange. If several displacement transducers are available, their output can be used without further complications introduced by the uncertainty of wavelength and wave location. It should be noted that the quantity $\overline{A_1}\sin(\pi x/L)$ will be very

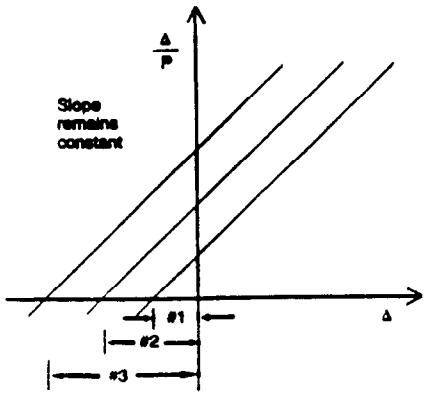

Fig. 5. Linearized plot showing slope independence with respect to dial gauge placement.

small due to the fact that the initial deflection is not apparent in the column, but initial imperfections in the material exist. It should also be noted that in the extreme case when little or no measurement is recorded, the gauge may be positioned at inflection point $x = 0$ or L. In this case, the measurements taken from the gauge should be neglected for the Southwell analysis.

4 ANALYSIS OF EXPERIMENTS

Local flange buckling of an axially compressed column plays an important role in the load carrying capacity of the member. Since deformations in the flange during local buckling can be quite large, they can induce material damage. Therefore, the local buckling load can be used as a failure criterion for the entire column.

In this section, the local flange buckling behavior of pultruded composite wide flange I-beams is studied. A theoretical orthotopic plate model based on the Levy method with one free and one elastically restrained edge was used to predict the behavior of the test specimens.[6] For each section being tested, three cases were considered for the elastic spring constant d representing the amount of elastic support provided by the web: clamped ($d \to \infty$), elastic ($d = D_{22}^{\text{WEB}}$) and hinged ($d = 0$). As shown by Raftoyiannis,[15] the elastic supported boundary condition $d = D_{22}^{\text{WEB}}$ best approximates the true boundary conditions which exist in the wide flange I-beam. Thus, any experimental loads will be compared to the elastically restrained case.

In addition to the theoretical curves, numerous experimental tests were performed on each wide flange I-beam section. At least three tests were done on each section with lengths corresponding to mode II, III and IV of the theoretical local buckling curves. Dial gauges were placed along the flanges and measurements of the flange deflection and load were obtained. A scheme based on Southwell's method, as described in Section 3, was used to reduce the data and determine the critical load. All experimental loads appear to be in good agreement with the theoretical predicted value.

4.1 Experimental setup and procedure

The flange local buckling tests were performed using a Baldwin test machine to apply the axially compressive load to the specimens. Various column lengths were cut, depending on the specific section being tested. The FRP beam specimens were manufactured and supplied by Creative Pultrusions, Inc.[1] Local buckling tests were conducted using the following

doubly-symmetric wide flange I-beams: 102 mm × 102 mm × 6·4 mm (4″ × 4″ × 1/4″); 152 mm × 152 mm × 6·4 mm (6″ × 6″ × 1/4″); 152 mm × 152 mm × 9·5 mm (6″ × 6″ × 3·8″) and 203 mm × 203 mm × 9·5 mm (8″ × 8″ × 3/8″). Table 1 shows the flange properties for each FRP section along with the elastic support provided by the web. Using the properties for each section, Figs. 6–9 show the theoretical buckling curves predicted by the Levy solution[6] along with the overall (Euler) buckling curves. Note that in Figs 6–9, the plots were nondimensionalized by the flange width and the local buckling load (listed below in Tables 2–4) for each section.

Since all the lengths and sections were to be loaded into compression, it was very important to check that all cuts made were perpendicular to the column length. This was done to ensure that the cross-section was loaded uniformly.

To distribute a uniform load from the Baldwin machine, a thick steel plate was used at both ends. In addition to the steel plate, a protective grid constructed from 25·4 mm (1″) steel square bar was mounted to the plate.

TABLE 1

Flange Properties and Web Support for Each Wide-Flange I-Beam Section (note: $D_{16} = D_{26} = 0$ for all flanges

Section (mm)	D_{11} *(N cm) [×10³]*	D_{12} *(N cm) [×10³]*	D_{22} *(N cm) [×10³]*	D_{66} *(N cm) [×10³]*	D_{22}^{WEB} *(N cm) [×10³]*
102 × 102 × 6·4	45·04	8·218	20·88	6·664	20·74
152 × 152 × 6·4	48·46	9·121	22·92	7·248	21·05
102 × 102 × 9·5	157·1	26·71	68·71	22·23	67·11
203 × 203 × 9·5	161·3	26·82	69·09	22·39	67·52

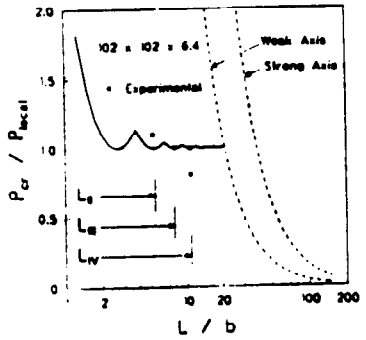

Fig. 6. Experimental loads for modes II, III and IV compared with theoretical curves for the 102 mm × 102 mm × 6·4 mm (4″ × 4″ × 1/4″) WF I-beam.

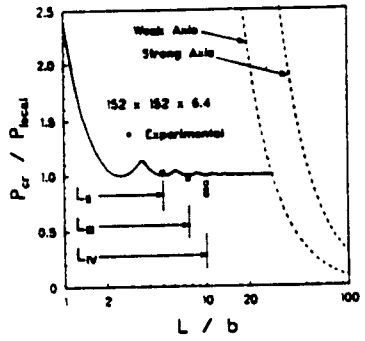

Fig. 7. Experimental loads for modes II, III and IV compared with theoretical curves for the 152 mm × 152 mm × 6·6 mm (4" × 6" × 1/4") WF I-beam.

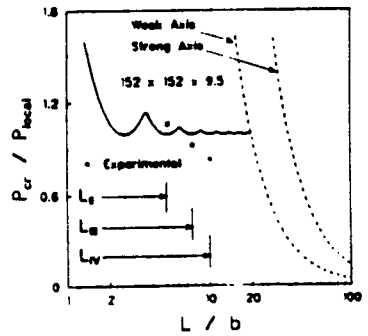

Fig. 8. Experimental loads for modes II, III and IV compared with theoretical curves for the 152 mm × 152 mm × 9·5 mm (6" × 6" × 3/8") WF I-beam.

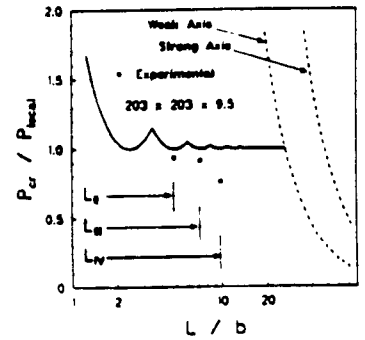

Fig. 9. Experimental loads for modes II, III and IV compared with theoretical curves for the 203 mm × 203 mm × 9·5 mm (8" × 8" × 3/8") WF I-beam.

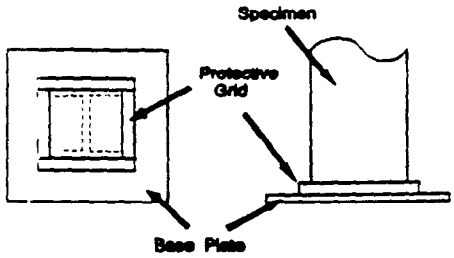

Fig. 10. Experimental setup showing base plate and protective grid.

This protective grid surrounds the specimen on all sides, as shown in Fig. 10, to protect against lateral slippage. It should be noted that the protective grid does not allow free rotation at the ends of the column but was needed for safety reasons. Hence, the boundary conditions are slightly different than the simply supported case assumed in the theoretical analysis.

Dial gauges, with 0·025 mm (0·001") accuracy and a maximum measurement of 25·4 mm (1"), were used to detect the deflection of the flanges. An average of four dial gauges were placed along the specimen length attached to the outer edge of the flange. Figure 11 shows a typical dial gauge placement along the specimen length. As seen from Fig. 11, the dial gauges were staggered on both sides of the flanges along the length of the column. Since the exact shape and mode of the deflected flange are unknown, the exact longitudinal placement of the gauges was determined randomly in a staggered pattern as indicated above. All dial gauges were then placed into position and preset to a reading of approximately 12·7 mm (0·5"). This presetting was done to allow the deflection of the flange to be positive or negative, as measured by the dial gauge, since the shape, inflection and mode of the flange is an unknown.

The testing procedure consisted of loading the column and periodically taking measurements from the dial gauges. In the initial phases of the tests, the stepsize of the readings somewhat depended upon the theoretically predicted local buckling load (22 kN to 44 kN stepsize). Once a noticeable change occurred in the gauges, the stepsize in the gauge readings was decreased. It was also noticed that in the very initial stages of the tests ($P < 111$ kN), the gauge readings fluctuated slightly. These changes are not considered as buckling, but as deformations occurring while the column was being loaded as a result of initial imperfections. Once a certain load was reached (around $P = 120$ kN), the gauges stabilized and did not move until the approach of the local buckling load. It should be noted that these initial imperfections were not consistent in all specimens

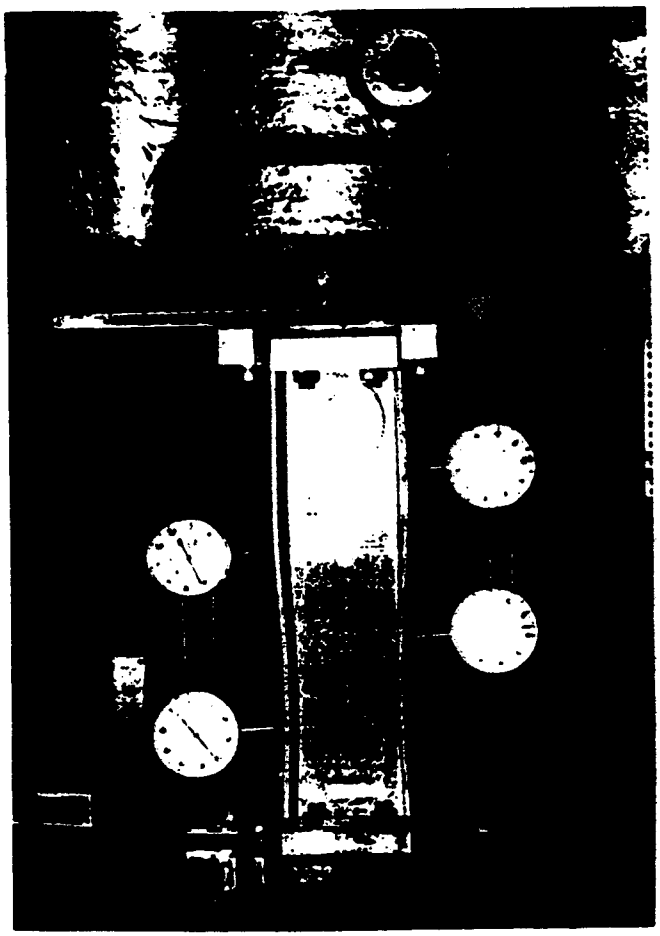

Fig. 11. Typical dial gauge placement along WF I-beam flanges (actual test shown for the 102 mm × 102 mm × 6·4 mm (4" × 4" × 1/4") WF I-beam).

that were tested (some specimens stabilized at or below 22 kN). All specimens stabilized over an ample range of loads (133 kN to 445 kN range). Hence, all measurements taken before the stabilized period were neglected for the buckling analysis.

Almost all specimens were loaded and measurements taken until the flange was clearly buckled by eyesight. Once the final readings were taken, the column was unloaded. It should also be noted that in most tests, cracking of various kinds occurred inside the columns during the test. Thus, any attempt to reload the specimen to repeat the test will result in lower readings for the local buckling load than in the initial test when the material is undamaged.

4.2 Experimental test results

Local flange buckling tests were conducted on the wide flange I-beams listed in Section 4.1. At least three tests were done on each section. The lengths that were tested corresponded to the theoretical length calculated for a local buckling mode of II, III and IV. During each test, dial gauge measurements were taken from each gauge. The results were then plotted on a Δ–P plot, in which a hyperbolic relation was obtained (see Section 2). This curve was then linearized on a Δ–Δ/P, in which a linear regression was done on each separate gauge measurement (see Section 3). The average correlation coefficient calculated for each gauge measurement for all local buckling tests was 0·99. The resulting slopes and intercepts (regression coefficients) were averaged to obtain a general slope for the test. The resulting critical buckling load was then determined from the inverse of the average slope. The deviation of the average regression line with respect to the individual regression line for a single gauge (for each single test) was less than 1% for all tests. Hence, averaging of the slopes obtained from each gauge introduced a negligible error in the buckling load. For plotting purposes, the intercepts were also averaged in order that all gauge measurements and the average regression line could be shown on a single plot for one local buckling test. The average intercept for the test introduced virtually no change in any regression line with respect to the original line due to the extremely small magnitude of the intercept value (small imperfection).

4.2.1 Mode II results

The shortest lengths that were tested in the short column tests were lengths corresponding to a local buckling mode II. For the theoretical mode II lengths, the buckled flange will have a shape corresponding to two full wavelengths. Figures 6–9 show the mode II lengths as determined from each of the theoretical curves generated in Section 4.1, corresponding to each wide flange I-beam. Figures 12–14 show the gauge measurements taken during the test and the resulting linear regressed line corresponding to three of the wide flange I-beam sections tested. These three examples show the behaviors observed throughout the experimental program. As seen from Figs 12–14, all gauge measurements have a hyperbolic relationship and a resulting linear relationship for Δ and Δ/P. The extent of the hyperbolic relationship was dependent on the amount of imperfection existing in the material and varied from test to test. Table 2 shows the length, theoretical buckling load, experimental buckling load (inverse of the slope) and the percentage difference between the theoretical and

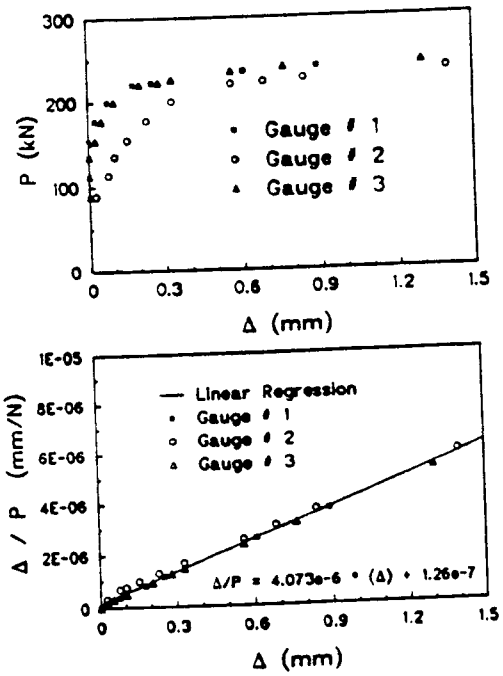

Fig. 12. Mode II hyperbolic and linearized measurements for the 102 mm × 102 mm × 6·4 mm (4" × 4" × 1/4") WF I-beam.

experimental loads for each section tested. As seen from Table 2, the percentage error is less than 11% for all sections tested. With the exception of the 203 mm × 203 mm × 9·5 mm (8" × 8" × 3/8"), which may be due to a large imperfection, all experimental loads are slightly higher than the theoretical value. This larger load and percentage error obtained could be a direct result of the boundary conditions assumed in the theoretical analysis. As stated before, the theoretical analysis[6] assumes simply-supported boundary conditions at the ends. The boundary conditions in the test were not simply-supported but a combination of fixed and simply-supported. This boundary condition difference can explain the higher load obtained experimentally.

4.2.2 Mode III results

The next lengths that were tested corresponded to mode III lengths, shown in Figs 6–9, as taken from the theoretical curves for each section tested. For the theoretical mode III lengths, the buckled flange will have a shape corresponding to three full wavelengths. Figure 15 shows the hyperbolic measurements taken during the test of the

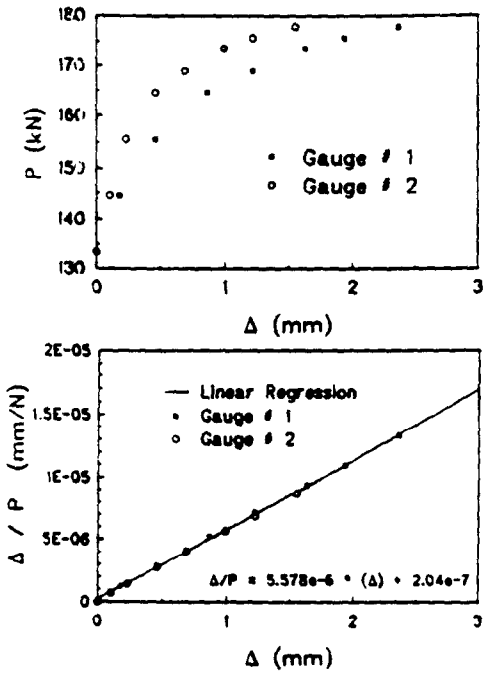

Fig. 13. Mode II hyperbolic and linearized measurements for the 152 mm × 152 mm × 6·4 mm (6" × 6" × 1/4") WF I-beam.

TABLE 2
Resulting Experimental Local Buckling Loads for Mode II Tests

Section (mm)	*Length (cm)*	P_{theory} *(kN)*	$P_{exper.}$ *(kN)*	*% Diff.*
102 × 102 × 6·4	26·7	223·5	246·6	10·3
152 × 152 × 6·4	38·1	175·3	179·0	2·1
152 × 152 × 6·4	38·1	175·3	179·3	2·3
152 × 152 × 9·5	39·4	547·5	583·9	6·7
203 × 203 × 9·5	49·5	434·4	406·1	6·5

152 mm × 152 mm × 6·4 mm (6" × 6" × 1/4") wide flange I-beam and the resulting linear regressed line. Table 3 shows the length, theoretical buckling load, experimental buckling load (inverse of slope) and the percentage difference between experimental and theoretical loads. As seen in Table 3, all differences were less than 9% and all loads were slightly lower than the theoretical (which could result from material imperfection). It should also be noted that both the 102 mm × 102 mm × 6·4 mm (4" × 4" × 1/4") and the 152 mm × 152 mm × 6·4 mm (6" × 6" × 1/4") tests result in errors less than 4%, thus proving the accuracy of the theoretical values.

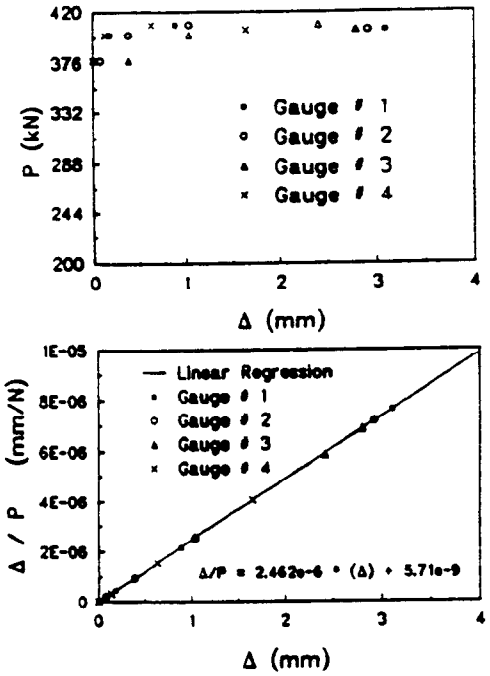

Fig. 14. Mode II hyperbolic and linearized measurements for the 203 mm × 203 mm × 9·5 mm (8" × 8" × 3/8") WF I-beam.

TABLE 3
Resulting Experimental Local Buckling Loads for Mode III Tests

Section (mm)	*Length (cm)*	P_{theory} *(kN)*	$P_{exper.}$ *(kN)*	*% Diff.*
102 × 102 × 6·4	40·6	223·5	223·6	0·0
152 × 152 × 6·4	57·2	175·3	170·4	2·8
152 × 152 × 6·4	57·2	175·3	169·1	3·6
152 × 152 × 6·4	57·2	175·3	174·3	0·6
152 × 152 × 9·5	58·4	547·5	507·2	7·3
203 × 203 × 9·5	73·7	434·4	396·8	8·7

4.2.3 Mode IV tests

The longest columns that were tested in the short column range were those corresponding to mode IV, shown in Figs 6–9, of the theoretical curves. For the theoretical mode IV lengths, the buckled flange will have a shape corresponding to four full wavelengths. Figure 16 shows the hyperbolic measurements taken during the test of the 152 mm × 152 mm × 6·4 mm (6" × 6" × 1/4") wide flange I-beam and the resulting regressed line. Table

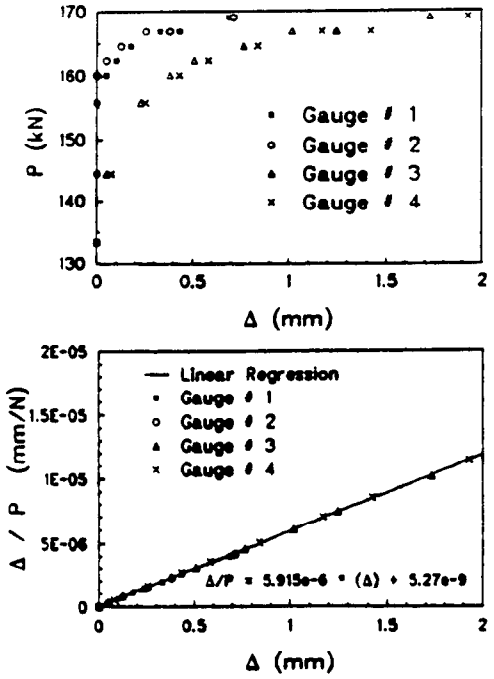

Fig. 15. Mode III hyperbolic and linearized measurements for the 152 mm × 152 mm × 6·4 mm (6" × 6" × 1/4") WF I-beam.

4 shows the length, theoretical buckling load, experimental buckling load (inverse of slope) and the percentage difference between the theoretical solution and the experimental results. As seen from Table 4, all percentages are rather large (13–24%) and all loads are below the theoretical prediction. These large differences may be a result of interaction between long and short column ranges as shown by Tomblin.[16] The possibility of interaction can be visualized in Figs 6–9 from the length of the column in mode IV being close to the column length at the intersection of the local and Euler buckling curves.

4.3 Experimental observations

During the testing and data reduction procedure, various observations were made as follows:

(1) All gauges had small movements from the initial application of load and then stabilized at a load ($P \leq 111$ kN) until flange buckling occurred. The stable range was large (133 kN to 445 kN).
(2) In several cases one flange buckled before the other, which may be

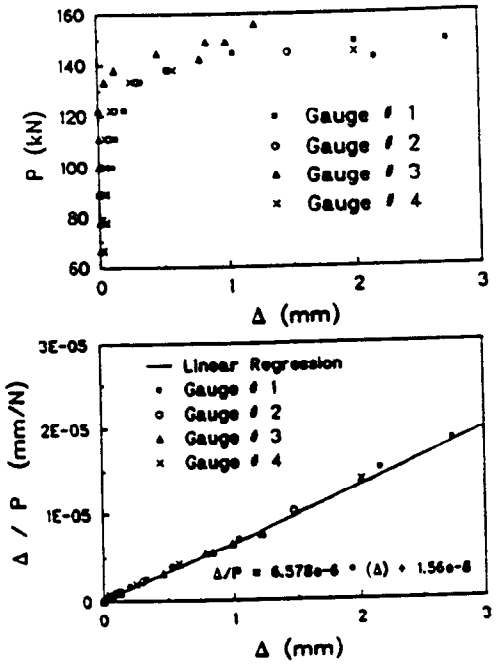

Fig. 16. Mode IV hyperbolic and linearized measurements for the 152 mm × 152 mm × 6·4 mm (6" × 6" × 1/4") WF I-beam.

TABLE 4
Resulting Experimental Local Buckling Loads for Mode IV Tests

Section (mm)	*Length (cm)*	P_{theory} *(kN)*	$P_{exper.}$ *(kN)*	*% Diff.*
102 × 102 × 6·4	54·6	223·5	180·8	19·1
102 × 102 × 6·4	54·6	223·5	222·4	5·0
152 × 152 × 6·4	76·2	175·3	143·0	18·4
152 × 152 × 6·4	76·2	175·3	148·8	15·1
152 × 152 × 6·4	76·2	175·3	161·8	7·7
152 × 152 × 6·4	76·2	175·3	152·0	13·3
152 × 152 × 9·5	77·5	547·5	455·3	16·8
203 × 203 × 9·5	100·3	434·4	329·2	24·2

caused by imperfections existing in that flange. However, this phenomenon did not affect the value of the critical load due to the use of the data reduction method proposed herein.

(3) When flange buckling occurred, all gauges had movement without extra addition of load. Thus, possible human error in gauge readings may exist. However, the dispersion of values and correlation with theoretical prediction are very good.

(4) In the case of the 152 mm × 152 mm × 9·5 mm (6″ × 6″ × 3/8″) and the 203 mm × 203 mm × 9·5 mm (8″ × 8″ × 3/8″) sections, only a few gauge readings could be obtained. This was due to the fact that once buckling occurred, the column experienced loud cracking and large gauge movements. This, in combination with the high load, made the total failure of the column progress very quickly and made manual reading of the gauges difficult.

(5) During the testing procedure, in the case in which no changes in the gauge readings are obtained (i.e., gauge positioned at an inflection point), the gauge readings must be neglected in the regression analysis. However, during all the testing done on all the FRP sections, this was encountered only twice.

(6) Mode IV tests produced the highest degree of error between experimental loads and theory. These discrepancies are due to interaction existing between the local and global buckling modes as shown by Tomblin.[16]

(7) Although the proposed method accurately determines the local buckling of the flange, all FRP columns tested exhibited a certain degree of post-buckling stiffness. Hence, the total ultimate strength of the column is greater than that predicted by just the local buckling analysis. However, it should be noted that in most cases, permanent damage of the section occurred via internal cracks, delamination, etc., as was evident when the column was reloaded.

(8) Due to the instrumentation employed, no measurement of the post-buckling wavelength was possible.

Figures 6–9 show the experimental load obtained plotted with the theoretical curves for each section. As seen from these figures, good agreement with the elastically restrained theoretical load exists.

5 CONCLUSIONS

The local flange buckling load obtained experimentally appears to be in good agreement with the theoretical loads for each wide flange I-beam section tested. As shown in Tables 2 and 3, all percentage differences between the theoretical and experimental loads are below 11%. The large percentage differences experienced in the mode IV test reported in Table 4 should be further investigated. Measurements of the post-buckling wavelength should be attempted.

A novel method to obtain the local buckling load based on Southwell's method was developed. As can be seen in the linearized Δ–Δ/P plots, all

measurements fall close to the regressed straight line with very little data scatter. Thus, by using this method in local buckling tests of pultruded beams, one can account for the material imperfections common in the pultrusion manufacturing process.

ACKNOWLEDGEMENTS

This research was supported by Creative Pultrusions, Inc. The materials used in this investigation were supplied by the same company. Their collaboration is gratefully acknowledged. The help of technicians in the College of Engineering at West Virginia University is also appreciated.

REFERENCES

1. *Creative Pultrusions Design Guide.* Creative Pultrusions, Inc., Pleasantville Industrial Park. Alum Bank, PA 15521, 1988.
2. Chajes, A., *Principles of Structural Stability Theory.* Prentice-Hall, Englewood Cliffs, NJ, 1974.
3. Jones, R. M., *Mechanics of Composite Materials.* Hemisphere Publishing Corporation, New York, 1975.
4. Tsai, S. W. & Hahn, H. T., *Introduction to Composite Materials.* Technomic Publishing Co., Lancaster, PA, 1980.
5. Barbero, E. J., Pultruded structural shapes — from the constituents to the structural behavior. *SAMPE J.*, 27(1) (1991) 25–30.
6. Barbero, E. J. & Raftoyiannis, I. G., Buckling analysis of pultruded composite columns. In *Impact and Buckling of Structures*, ed. D. Hui & I. Elishakoff, ASME, AD-Vol. 20, AMD-Vol. 114, 1990, 47–52.
7. Bleich, F., *Buckling Strength of Metal Structures.* McGraw-Hill, New York, 1952.
8. Cheung, Y. K., *Finite Strip Method in Structural Analysis.* Pergamon Press, New York, 1976.
9. Vakiener, A.R., Zureick, A. & Will, K. M., Prediction of local flange buckling in pultruded shapes by finite element analysis. *Advanced Composite Materials*, ASCE Publications, 1991, pp. 302–12.
10. Yuan, R. L., Hashen, Z., Green, A. & Bisarnsin, T., *Fiber-reinforced plastic composite columns.* In *Advanced Composite Materials in Civil Engineering Structures*, ed. S. L. Iyer, ASCE, Las Vegas, NV, 31 January–1 February 1991, pp. 205–11.
11. Southwell, R. V., On the analysis of experimental observations in problems of elastic stability. *Proc. Roy. Soc. London (A)*, **135** (1932) 601–16.
12. Southwell, R. V., *Theory of Elasticity.* Oxford University Press, London, 1941.
13. Tsai, W. T., Note on Southwell's method for buckling tests of struts. *J. Appl. Mech.*, **53** (1986) 953–4.

14. Fisher, H. R., An extension of Southwell's method of analyzing experimental observations in problems of elastic stability. *Proc. Roy. Soc. London (A)*, **144** (1934) 609–30.
15. Raftoyiannis, I. G., *Buckling of Pultruded Composite Columns*. MSCE Thesis, West Virginia University, WV, 1991.
16. Tomblin, J. S., *A Universal Design Equation for Pultruded Composite Columns*. MSME Thesis, West Virginia University, WV, 1991.

Thin-Walled Structures 18 (1994) 117–131

A Phenomenological Design Equation for FRP Columns with Interaction between Local and Global Buckling

Ever Barbero & John Tomblin

Mechanical and Aerospace Engineering, Constructed Facilities Center, West Virginia University, Morgantown, WV 26506-6101, USA

(Received 15 June 1992; revised version received 7 December 1992; accepted 15 March 1993)

ABSTRACT

A design equation for fiber reinforced plastic columns is presented in this paper, based on the interaction between local (flange) and global (Euler) buckling observed during testing of the FRP columns included in this investigation. An existing interaction equation is adapted to account for the modes of failure observed in columns made of fiber reinforced composite materials. Experimental data generated during this investigation are presented and used to validate the interaction equation and to obtain the interaction constant. A slenderness ratio is proposed and used to present a plot of buckling for all sections and column lengths (short, long, and intermediate). An expression for the optimum column length to be used in the experimental determination of the interaction constant is proposed.

1 INTRODUCTION

Pultruded composite beams and columns are being used for civil engineering structural applications[1] and aerospace applications.[2] Composite materials have many advantages over conventional materials (steel, concrete, wood, aluminum, etc.), such as light weight and high corrosion resistance. Mass production of composite structural members (e.g. by pultrusion) makes composite materials cost-competitive with conventional ones.

In the pultrusion process, fibers impregnated with a polymer resin are

Thin-Walled Structures 0263-8231/94/$07·00

pulled through a heated die that provides the shape of the cross-section to the final product. Pultrusion is a continuous process for manufacturing prismatic sections of virtually any shape.[3] Other mass-production techniques like automatic tape layout can also be used to produce prismatic sections.

Pultruded structural members have open or closed thin-walled cross-sections. For long composite columns, global (Euler) buckling is expected to occur before any other instability failure. The buckling equation has to account for the anisotropic nature of the material. Theoretical predictions correlate well with experimental data for long columns.[4] For short columns, local buckling occurs first, leading either to large deflections and finally to overall buckling, or to material degradation due to large deflections (crippling). Because of the large elongation of failure allowed by both the fibers and the resin, the composite material remains linearly elastic for large deflections and strains, unlike conventional materials that yield (steel) or crack (concrete) for moderate strains. Therefore, buckling is the governing failure for this type of cross-section and the critical buckling load is directly related to the load carrying capacity of the member. Theoretical predictions for short column buckling taking into account the anisotropy of the material correlate well with experimental observations.[5–7]

The experimental data for short and long column buckling[4–7] suggest the existence of an intermediate-column region where the critical loads are lower than the predictions of both local and global buckling theories. Since fiber reinforced plastics (FRPs) remain linearly elastic for large values of strain, buckling in the intermediate range occurs due to mode interaction between the local (flange) and global (Euler) buckling modes rather than between local buckling and yield as in the case of steel columns. Mode interaction has been shown by Arbocz[8] to reduce the buckling load. In this paper, a phenomenological design equation is presented to represent the buckling envelope for pultruded composite I-beams. The formulation accounts for the interaction between local (flange) and global (Euler) buckling modes. In the formulation, an adjustable interaction parameter was used to also account for various material imperfections and interaction levels apparent in pultruded members. The interaction constant is determined through a series of tests described in this paper.

2 STEEL INTERACTION CURVES

Experimental data on steel columns deviate from predictions based on Euler's column buckling formula due to inelastic behavior of the material

in the short to intermediate column range. Considère[9] and Engesser[10] developed a theory for inelastic buckling in the short to intermediate column range. The tangent modulus theory states that Euler's formula would be valid if the modulus of elasticity E were replaced by the tangent modulus of elasticity E_t. In this theory, it is assumed that the bending stress distribution due to buckling adds to the uniform compressive stress in the column. Engesser[11] proposed a second theory, the double modulus theory or reduced modulus theory, which states that the modulus of elasticity E in Euler's formula must be replaced by a reduced modulus E_r which is a function of the tangent modulus, the elastic modulus, and the moments of inertia on each side of the neutral axis. In this theory, the tangent modulus E_t should be used on the concave side and the elastic modulus E on the convex side where stresses relax due to bending.

Bleich[12] compares the reduced modulus and tangent modulus theories with experimental results, showing that the experimental loads fall below the critical load predicted by the reduced modulus theory and closer to the tangent modulus theory. Shanley[13] showed that columns start to deflect at a load significantly below the load predicted by the reduced modulus theory. These deflections occur in combination with an increasing axial load. Thus, Shanley concluded that the tensile strain increments caused by the deflection are compensated by the axial shortening of the column. Hence, there is no stress-relaxation anywhere in the cross-section. Shanley goes further to conclude that the maximum load of the column lies somewhere between the tangent modulus load and reduced modulus load.

The tangent and reduced modulus theories can physically explain the inelastic buckling of short and intermediate columns but are rather cumbersome from a design standpoint due to the variability of the tangent modulus with stress. Hence, design of column members is simplified by the use of empirical formulations.

According to the recommendations of the Column Research Council (CRC),[14,15] a single curve is used to model the mean trend of various types of columns. On the CRC curve, the critical stress is plotted against column slenderness. This design curve can be nondimensionalized by plotting σ_{cr}/σ_y against a universal slenderness ratio $\lambda_c = L/\rho(\sigma_y/\pi^2 E)^{1/2}$. The CRC curve is given by

$$\begin{aligned} &\text{For} \frac{L}{\rho} < c \quad \sigma_{cr} = \sigma_y \left[1 - \frac{1}{2c^2}\left(\frac{L^2}{\rho^2}\right)\right] \\ &\text{For} \frac{L}{\rho} \geq c \quad \sigma_{cr} = \frac{\pi^2 E}{(L/\rho)^2} \end{aligned} \tag{1}$$

where $c = (2\pi^2 E/\sigma_y)^{1/2}$. The equation does not reflect any safety factors or particular restrictions which may be implied by specific design codes.

3 WOOD INTERACTION CURVES

Column design equations for wood members are usually viewed as empirical equations for the compressive strength as a function of slenderness. Zahn[16] develops a column design equation for timber columns by viewing column failure as the interaction between crushing and buckling. In his analysis, Zahn uses the Ylinen[17] equation to model the interaction and develop a universal design equation. Zahn compares the Ylinen column design formulation with other column design equations such as Rankine–Gordon, Perry–Robertson, Neubauer and the fourth-power parabola formulations (reviewed in detail by Zahn[16]). In the Ylinen equation, the parameter c can be viewed as controlling the amount of interaction between crushing and global (Euler) buckling. Zahn states that the parameter c accounts for the effects of nonlinear compression and inhomogeneity of the material. Zahn goes further to state that the parameter c may also be used to automatically include the effect of crookedness as long as the column test specimens are randomly selected from an appropriate sample of columns. Due to its versatility, the Ylinen equation surpasses other empirical equations in which all interaction is assumed to be equivalent to load eccentricity.

The column design equation presented by Zahn is

$$r = \frac{1 + 1/\lambda^2}{2c} - \sqrt{\left(\frac{1 + 1/\lambda^2}{2c}\right)^2 - \frac{1}{c\lambda^2}} \tag{2}$$

where

$$r = \frac{\text{actual strength}}{\text{rupture strength}} \tag{3}$$

and λ is a universal slenderness ratio, independent of material properties, defined as

$$\lambda = \frac{1}{\pi}\frac{L}{\rho}\sqrt{\frac{F_c}{E}} \tag{4}$$

where F_c is the compressive strength. Note that by this definition

$$\lambda^2 = \frac{s}{r} \tag{5}$$

where

$$s = \frac{\text{actual strength}}{\text{buckling strength}} \tag{6}$$

This shows that slenderness is the controlling parameter in the interaction of the two modes.

Note that by the definition of r and s, linear interaction is defined as

$$r + s = 1 \tag{7}$$

Linear interaction is a conservative approximation for design purposes. But using available column data, Zahn points out that the sum of r and s should exceed one. Thus, another term is added to eqn (7). In order to preserve symmetry, the product of r and s is added, and eqn (7) becomes

$$r + s = 1 + crs \tag{8}$$

Equation (8) models linear interaction if $c = 0$ and the noninteraction case if $c = 1$. Interaction between crushing and Euler buckling results in an intermediate value of c to be found experimentally. This equation was presented first by Ylinen[17] and later adopted by Zahn[16] to model wood columns; Zahn also proposed to interpret c as an interaction parameter.

4 PULTRUDED I-BEAM INTERACTION CURVES

Unlike wood and steel, FRPs remain linear for large values of strain. The interaction occurs between local and global modes unless the column is so short that material crushing also occurs. Following the approach of Zahn,[16] a phenomenological column design equation for pultruded I-beams is developed to account for the interaction between the local and global buckling observed in this experimental program. The buckling strength ratios q and s are defined as follows:

$$q = \frac{\text{actual failure load}}{\text{local buckling load}} = \frac{\text{actual strength}}{\text{local buckling strength}} \tag{9}$$

$$s = \frac{\text{actual failure load}}{\text{Euler buckling load}} = \frac{\text{actual strength}}{\text{Euler buckling strength}} \tag{10}$$

Equation (8) can now be applied to represent interaction of local and global modes in FRP columns (note that q replaces r in Zahn's formulation). The controlling parameter c is used to model the amount of interaction between local (flange) buckling and global (Euler) buckling. In the limiting cases, if $c = 0$ linear interaction results, and if $c = 1$ the case of noninteraction is recovered (Fig. 1).

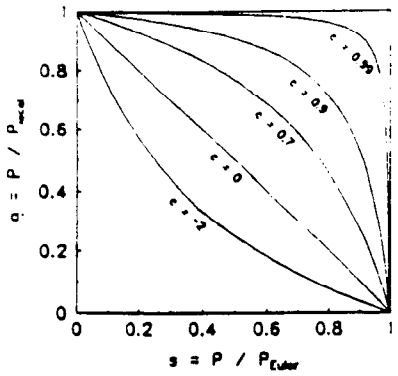

Fig. 1. Various values for the interaction constant c.

A universal slenderness ratio for pultruded I-beam columns can be defined as

$$\lambda = kL\sqrt{\frac{P_{\text{local}}}{D\pi^2}} \tag{11}$$

where k is the effective length coefficient, L is the column length, D is the bending stiffness and P_{local} is the theoretical local buckling load. The effective length coefficient k is given by analytical formulation for columns with various end conditions found in many strength of materials textbooks and design manuals. Since $P_{\text{Euler}} = \pi^2 D/L^2$, using eqn (11) we obtain $P_{\text{Euler}} = P_{\text{local}}/\lambda^2$ which when substituted into eqn (8) gives

$$c\lambda^2 q^2 - (1 + \lambda^2)q + 1 = 0 \tag{12}$$

The root of this equation is

$$q = \frac{P_{\text{cr}}}{P_{\text{local}}} = \frac{1 + 1/\lambda^2}{2c} - \sqrt{\left(\frac{1 + 1/\lambda^2}{2c}\right)^2 - \frac{1}{c\lambda^2}} \tag{13}$$

which represents actual values of q determined experimentally and described by the interaction parameter c with λ given by eqn (11). Therefore, eqn (13) can be used as a design equation over the entire range of column slenderness, short, intermediate, and long. The bending stiffness D of a FRP column is computed from the information provided by the manufacturer for each section following the methodology developed by Barbero[18] for pultruded composite beams. This information includes the type of fibers and matrix material, the local and orientation of the fibers and the fiber content in the cross-section (Fig. 2). Table 1 shows the flange and web bending stiffness components for a 102 mm × 102 mm × 6·4 mm (4″ × 4″ × 1/4″) and 152 mm × 152 mm × 6·4 mm (6″ × 6″ × 1/4″)

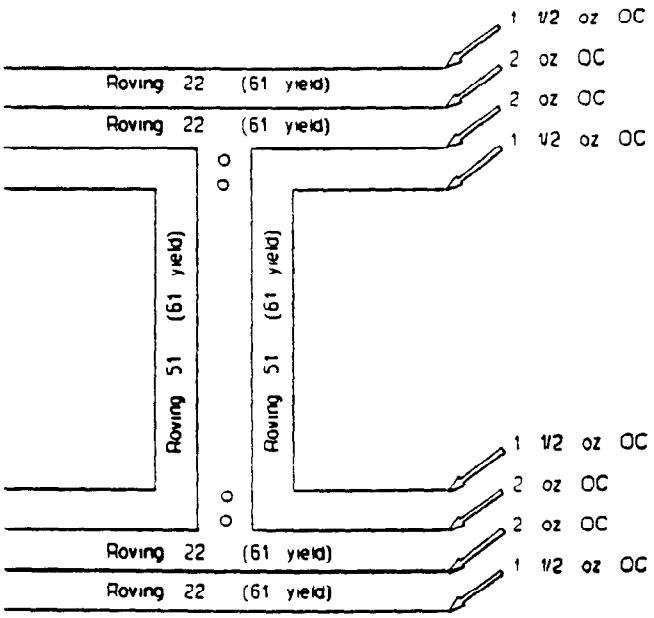

Fig. 2. Creative Pultrusions schematic for the 152 mm × 152 mm × 6·4 mm (6" × 6" × 1/4") WF I-beam.

pultruded WF I-beam, respectively, for bending about the weak axis. The local buckling loads were predicted based on the same information using the analysis presented by Barbero and Raftoyiannis[19]. The maximum interaction between local and global buckling occurs when $q = s$. Using $\lambda = 1$ in eqn (11), the column length for which maximum interaction occurs is

$$L^* = \frac{1}{k}\sqrt{\frac{D\pi^2}{P_{local}}} \tag{14}$$

TABLE 1
Weak Axis Bending Stiffness Components of the Flanges and Web for Each of the WF I-Beam Sections Tested (note: $D_{16} = D_{26} = 0$ for each section)

Stiffness Component	*102 mm × 102 mm × 6·4 mm*		*152 mm × 152 mm × 6·4 mm*	
	Flanges (M N-cm)	*Web (k N-cm)*	*Flanges (M N-cm)*	*Web (k N-cm)*
D_{11}	13·176	43·720	30·295	46·217
D_{22}	4·958	20·747	11·628	21·052
D_{12}	1·878	8·181	4·435	8·267
D_{66}	1·652	6·603	3·852	6·736

TABLE 2
Maximum Interaction Length L^* for Each Pultruded WF I-Beam Section

Section (mm)	L^* *(cm)*	P_{local} *(kN)*	D *(MN cm²)*
102 × 102 × 6·4	105·9	223·25	253·71
152 × 152 × 6·4	221·5	175·12	872·31

Table 2 shows the value of L^* along with the local buckling load and the weak axis bending stiffness D for each WF I-beam section considered in this paper. L^* corresponds to a length in which maximum interaction between local and global buckling is expected. Therefore, experimental data to obtain the interaction constant should be gathered at this length.

Using the universal slenderness ratio and the ratio of $q = P_{cr}/P_{local}$, the theoretical buckling envelopes for all WF I-beam sections can be collapsed into one universal curve (shaded area in Fig. 3).

5 EXPERIMENTAL RESULTS

The intermediate column tests were performed on the following pultruded WF I-beams: 152 mm × 152 mm × 6·4 mm (6″ × 6″ × 1/4″) and 102 mm × 102 mm × 6·4 mm (4″ × 4″ × 1/4″). More tests were done on

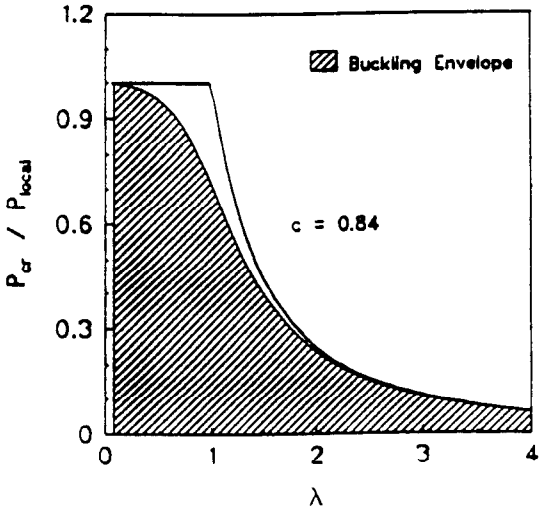

Fig. 3. Buckling envelope accounting for local–global buckling interaction.

the former I-beam because it has a wider range of lengths where interaction occurs. The testing procedure for the intermediate column lengths consisted of loading the specimen with controlled axial displacement. The load, the axial displacement, and the transverse deflection at the midspan were measured by a load cell and two LVDTs. The data was filtered from noise and recorded using a data acquisition system and a moving average technique.[20] The test was continued until the ultimate load of the column was achieved. The ultimate load was also recorded with a peak indicator on the Materials Testing System (MTS) control console. The data reduction simply consisted of obtaining the maximum load the column was capable of supporting, as recorded by the peak indicator on the MTS control console.

Since the span of the intermediate column range had not been previously established, the exact column lengths in the intermediate range were unknown. Hence, the testing lengths were taken between the longest local buckling test available and the shortest Euler buckling test previously performed.[4,21] All tests were conducted with the weak axis of the section in the pinned–pinned configuration. A larger number of samples correspond to lengths close to the predicted L^*. At lengths sufficiently far from L^*, only one test was done.

5.1 152 mm × 152 mm × 6·4 mm (6″ × 6″ × 1/4″) WF I-beam results

Intermediate column tests were performed on the pultruded 152 mm × 152 mm × 6·4 mm (6″ × 6″ × 1/4″) WF I-beam. An increased number of tests were performed around the value of L^* predicted in Table 2. The starting column length was 3·27 m (129″). This length was chosen due to the known Euler behavior apparent when testing a 3·58 m (141″) specimen.[4,21] Hence, column lengths were cut from 3·58 m (141″) progressively shorter in 30·5 cm (12″) increments.

Figure 4 shows the data acquired during the test of a 152 mm × 152 mm × 6·4 mm (6″ × 6″ × 1/4″) WF I-beam (deflection–load plot). Table 3 shows the lengths, theoretical local buckling load, theoretical Euler buckling load and maximum experimental load for each length tested. As seen in Fig. 4, once the maximum load was reached, the lateral deflection increased with decreasing compressive load, indicating a drastic loss of stiffness. As seen from Table 2, a significant decrease in critical load is obtained around the value of L^*. This indicates interaction between the local and global buckling modes. This interaction was also physically apparent during the test in which local flange buckling occurred in combination with lateral deflection. It must be noted that local–global interaction could be observed during the test because of the closely

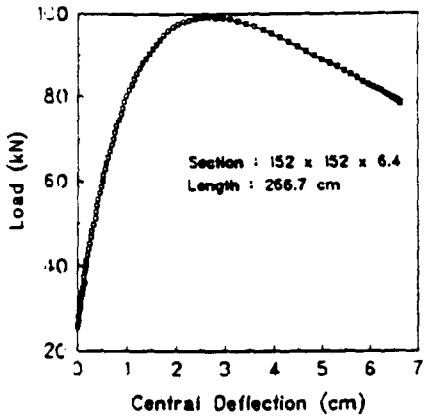

Fig. 4. Experimental intermediate test data on the 152 mm × 152 mm × 6·4 mm (6" × 6" × 1/4") WF I-beam (length = 266·7 cm).

controlled displacement of the column ends obtained by the servo-controlled actuator.

5.2 102 mm × 102 mm × 6·4 mm (4" × 4" × 1/4") WF I-beam results

Intermediate column tests were also performed on the pultruded 102 mm × 102 mm × 6·4 mm (4" × 4" × 1/4") WF I-beam. Since the range

TABLE 3
Experimental Intermediate Test Data on the 152 mm × 152 mm × 6·4 mm (6" × 6" × 1/4") WF I-Beam

Length (cm)	P_{local} *(kN)*	P_{Euler} *(kN)*	$P_{exper.}$ *(kN)*
144·8	175·33	418·00	174·34
175·3	175·33	280·23	148·99
175·3	175·33	280·23	157·23
175·3	175·33	280·23	151·15
175·3	175·33	280·23	156·45
205·7	175·33	203·38	136·83
205·7	175·33	203·38	133·06
205·7	175·33	203·38	138·18
236·2	175·33	152·64	116·67
236·2	175·33	152·64	115·40
236·2	175·33	152·64	120·10
266·7	175·33	121·03	99·23
297·2	175·33	97·48	78·19
327·7	175·33	80·18	67·13

TABLE 4
Experimental Intermediate Test Data on the 102 mm × 102 mm × 6·4 mm (4" × 4" × 1/4") WF I-Beam

Length (cm)	P_{local} *(kN)*	P_{Euler} *(kN)*	$P_{exper.}$ *(kN)*
114·3	223·52	191·68	171·08
114·3	223·52	191·68	161·98
147·3	223·52	115·39	98·53
147·3	223·52	115·39	95·29
177·8	223·52	79·21	71·58

on intermediate column is narrower than that of the 152 mm × 152 mm × 6·4 mm (6" × 6" × 1/4") WF I-beam (which is apparent from the theoretical curves), only three possible intermediate lengths were compatible with the testing frame. Therefore, only a limited number of tests were performed on this section with lengths closer to L^* (listed in Table 2) for which the maximum interaction between local and global buckling was expected.

Figure 5 shows the data acquired during the test of a 102 mm × 102 mm × 6·4 mm (4" × 4" × 1/4") WF I-beam (deflection–load plot). Table 4 shows the length, theoretical local buckling load and maximum experimental load for each column tested. As seen from Fig. 5, a loss of stiffness is also experienced at the maximum compressive load. As seen from Table 4, a decrease in the experimental load, when compared to theory, is also experienced, indicating interaction between the local and

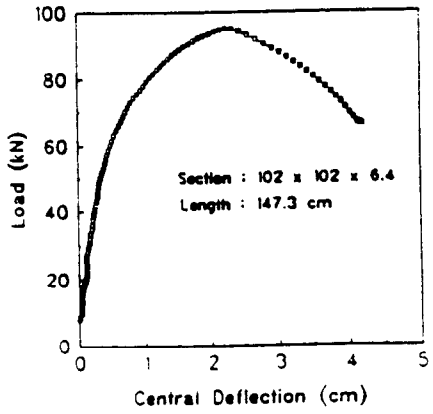

Fig. 5. Experimental intermediate test data on the 102 mm × 102 mm × 6·4 mm (4" × 4" × 1/4") WF I-beam (length = 147·3 cm).

global buckling modes. It was apparent during the test that both local buckling of the flanges and Euler buckling occurred simultaneously. These observations can be made because the test is not as catastrophic as a result of controlling the axial displacement with the hydraulic servo-controlled MTS.

6 DETERMINATION OF INTERACTION CONSTANT

Figure 6 shows the experimental interaction data plotted on an s versus q plot (P/P_{Euler} vs P/P_{local}) for the 152 mm × 152 mm × 6·4 mm (6" × 6" × 1/4") and 102 mm × 102 mm × 6·4 mm (4" × 4" × 1/4") pultruded WF I-beams. As seen from Fig. 6, symmetry appears to exist between the experimental failure loads. Thus, the use of eqn (8) as an interaction equation appears to be valid. Using the data in Tables 3 and 4, the interaction constant c was determined for the pultruded WF I-beam sections. The interaction constant physically describes the degree of interaction present between the local and global buckling failures. For each sample, the value of the interaction constant c was found by solving eqn (8) for c:

$$c = \frac{q + s - 1}{qs} \tag{15}$$

The interaction constant c for each type of cross-section was inferred from the experimental data by averaging the value of c of all samples. For the 152 mm × 152 mm × 6·4 mm (6" × 6" × 1/4") section, an interaction constant of $c = 0{\cdot}85$ was obtained. Similarly, for the 102 mm × 102 mm × 6·4 mm (4" × 4" × 1/4") section, an interaction

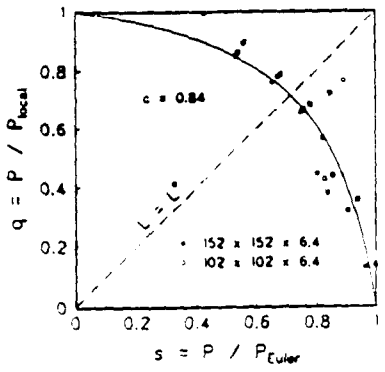

Fig. 6. Nondimensional q vs s plot for the combined interaction test data ($c = 0{\cdot}84$).

constant of $c = 0{\cdot}83$ was obtained. Comparing the values of the interaction constants, it seems that the interaction constant is independent of the size of the cross-section. However, additional I-beam sections should be tested to verify this result. Figure 6 also shows an average interaction constant of $c = 0{\cdot}84$ for both sections tested. As seen from the figure, the value of the interaction constant $c = 0{\cdot}84$ fits the experimental data obtained from the intermediate test.

Using the interaction constant c to approximate the interaction between local and global buckling, an overall buckling envelope is shown by the solid line in Fig. 7. Thus, it is proposed to use eqn (13) as a design equation for the buckling of pultruded composite I-beams. The buckling envelope shown by a solid line in Fig. 7 is valid for any pultruded I-beam section (similar to the sections used in this investigation) provided the values of the bending stiffness D, the local buckling load P_{local} and the interaction constant c are known. Also shown in the figure is additional experimental data obtained by Barbero and Tomblin[4] in the Euler column range. As seen in Fig. 7, the design equation closely approximates the true value of the failure load obtained in experiments.

Interaction is very pronounced for columns with lengths closer to L^*, as seen in the experiments. In this region, column failure occurs and rapidly induces large deformations and material failure (fiber breakage and delaminations). The importance of the interaction curve is evident from a design viewpoint. If the interaction value were not used, a difference of approximately 25% between the theoretically predicted local buckling load and the actual column failure load would be experienced at L^*. Furthermore, the proposed design equation is simpler to use than an Euler equation for long columns and a local buckling equation for short columns.

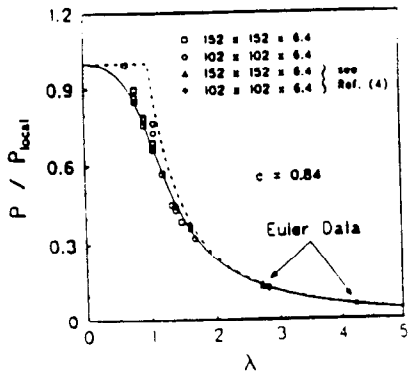

Fig. 7. Nondimensional q vs λ plot with intermediate and global buckling test data.

7 CONCLUSIONS

It is apparent that the design equation presented predicts well the actual critical loads of FRP columns of the type used in this investigation. The value of the interaction parameter $c = 0{\cdot}84$ provides a good estimate of the interaction between local and global buckling for the columns tested. The buckling envelope for pultruded composite WF I-beams shows good correlation with the experimental data developed in this investigation. Although more testing on other WF sections should be done in the future, the interaction curve and design envelope presented provide a basis for the design and use of pultruded structural members in engineering applications. Interaction of local and global buckling modes dominates the intermediate range of lengths of FRP columns used in this investigation. The definition of universal slenderness λ and buckling strength q proposed in this paper lead to a simple design equation to be used for the buckling of FRP columns.

The proposed design equation is based on a phenomenological approach. The interaction constant must be determined experimentally for each new section following the procedure presented in this work. All the sections used in this investigation can be described by the same value of the interaction constant. However, more experimentation is needed to determine if the interaction constant is independent of the cross-section. The validity of the proposed design equation for other types of sections not included in this investigation should be verified by additional experimentation. Development of a theoretical model for buckling mode interaction of FRP columns is underway.

ACKNOWLEDGEMENTS

This research was supported by Creative Pultrusions, Inc. The materials used in this investigation were supplied by the same company. Their collaboration is gratefully acknowledged. The help of the technicians in the College of Engineering at West Virginia University is also appreciated.

REFERENCES

1. GangaRao, H. V. S. & Barbero, E. J., Structural application of composites in construction. In *Encyclopedia on Composites*, ed. S. Lee, VCH Publications, New York, NY, 1991, Vol. 6, pp. 173–87.
2. Ashley, S., Advanced composites take flight. *Mechanical Engineering*, October 1991, 51–6.

3. *Creative Pultrusions Design Guide*. Creative Pultrusions, Inc., Pleasantville Industrial Park, Alum Bank, PA, 1988.
4. Barbero, E. J. & Tomblin, J. S., Euler buckling of thin-walled composite columns. *Thin-Walled Structures*, In Press. (1993).
5. Raftoyiannis, I. G., *Buckling of Pultruded Composite Columns*. MSCE Thesis, Department of Civil Engineering, West Virginia University, WV, 1991.
6. Tomblin, J. S. & Barbero, E. J., Local buckling experiments on FRP columns. *Thin-Walled Structures*, In Press. (1993).
7. Yuan, R. L., Hashen, Z., Green, A. & Bisarnsin, T., Fiber-reinforced plastic composite columns. In *Advanced Composite Materials in Civil Engineering Structures*, ed. S. L. Iyer, ASCE, Las Vegas, NV, 31 January–1 February 1991, pp. 205–11.
8. Arbocz, J., *Buckling and Postbuckling*. Springer-Verlag, Berlin, 1987.
9. Considère, A., Résistance des pièces comprimées. *Congrès International des Procédés de Construction*, Paris, 1891, Vol. 3.
10. Engesser, F., Ueber die Knickfestigkeit gerader Stabe. *Zeitschrift für Architektur und Ingenieurwesen*, Vol. 35, 1889.
11. Engesser, F., Knickgragen. *Schweitzerische Bauzeitung*, Vol. 26, 1895.
12. Bleich, F., *Buckling Strength of Metal Structures*. McGraw-Hill, New York, 1952.
13. Shanley, F.R., Inelastic column theory. *J. Aero. Sci.*, 14(5) (1947) 261.
14. Galambos, T. V., *Guide to Stability Design Criteria for Metal Structures*, Column Research Council, 4th edn. John Wiley, New York, 1988.
15. Bazant, Z. P. & Cedolin, L., *Stability of Structures*. Oxford University Press, New York, 1991.
16. Zahn, J. J., Re-examination of Ylinen and other column equations, interaction of rupture and buckling in wood members. *ASCE J. Struct. Eng.*, 118(10) (1992) 2716–28.
17. Ylinen, A., A method for determining the buckling stress and the required cross-sectional area for centrally loaded straight columns in elastic and inelastic range. *Publ. Int. Assoc. Bridge and Structural Engineering*, Zurich, Vol. 16, 1956.
18. Barbero, E. J., Pultruded structural shapes — from the constituents to the structural behavior. *SAMPE J.*, 27(1) (1991) 25–30.
19. Barbero, E. J. & Raftoyiannis, I. G., Buckling analysis of pultruded composite columns. In *Impact and Buckling of Structures*, ed. D. Hui & I. Elishakoff, ASME, New York, AD-Vol. 20, AMD-Vol. 114, 1990, pp. 47–52.
20. *Labtech Notebook* (version 6). Laboratory Technologies Corporation, Wilmington, MA, 1990.
21. Tomblin, J. S., *A Universal Design Equation for Pultruded Composite Columns*. MSME Thesis, Department of Mechanical and Aerospace Engineering, West Virginia University, WV, 1991.